Kicker Systems

M.J. Barnes
CERN, Geneva, Switzerland

Abstract

Each stage of an accelerator system has a limited dynamic range and therefore a chain of stages is required to reach high energy. A combination of septa and kicker magnets is frequently used to inject and extract beams from each stage. The kicker magnets typically produce rectangular field pulses with fast rise and/or fall times; however, the field strength is relatively low. To compensate for their relatively low field strength, the kicker magnets are generally combined with electromagnetic septa. The septa provide relatively strong field strength but are either DC or slow pulsed. This paper discusses injection and extraction systems with particular emphasis on the hardware required for the kicker system. Design options and computer aided design tools are also discussed. In addition, the interaction of the beam with the kicker system, primarily the kicker magnet, is considered.

Keywords

Injection; extraction; kicker; pulse power; beam coupling impedance; modulators.

1   Introduction

An accelerator stage has limited dynamic range: a chain of accelerator stages is required to reach high energy. Thus beam transfer into (injection) and out of (extraction) an accelerator is required. The design of the injection and extraction systems aims to achieve the following:

– minimize beam loss;

– place the newly injected or extracted particles onto the correct trajectory, with the correct phase space parameters.

A combination of septa and kickers is frequently used for injection and extraction. Septa can be electrostatic or magnetic: they provide slower field rise and fall times, but a stronger field, compared to kicker magnets. Some septa are designed to be operated with DC. Kicker magnets provide fast field rise and fall times, but relatively weak fields.

In general, a septum (plural: septa) is a partition that separates two cavities or spaces. In a particle accelerator, a septum is a device which separates two field regions. Important features of septa are an ideally homogeneous (electric or magnetic) field in one region, for deflecting the beam, and a low fringe field (ideally zero magnetic and electric field) next to the septum so as not to affect the circulating beam. Hence, a septum provides a space separation of circulating and injected/extracted beams. In contrast, a kicker magnet provides time selection (separation) of the beam to be injected/extracted: a kicker system is used for fast, single-turn, injection and extraction.

The processes of injection and extraction are covered in the proceedings of this CERN Accelerator School. The paper S*epta* discusses the hardware associated with septa. The present paper discusses the hardware associated with kicker magnets.

The field produced by a kicker magnet must rise/fall within the time period between the beam bunches (see sections 2 and 3). In addition, the magnetic field must not significantly deviate from the

flat top of the pulse or from zero between pulses (i.e., very small ripple/excursions): this is discussed further in the paper *Injection: Hadron Beams*, in the proceedings of this CERN Accelerator School. Typical field rise/fall times range from tens to hundreds of nanoseconds and pulse widths generally range from tens of nanoseconds to tens of microseconds. If a kicker exhibits a time-varying structure in the field pulse shape, this can translate into small offsets with respect to the closed orbit (betatron oscillations). Thus a fast, low-ripple, kicker system is generally required.
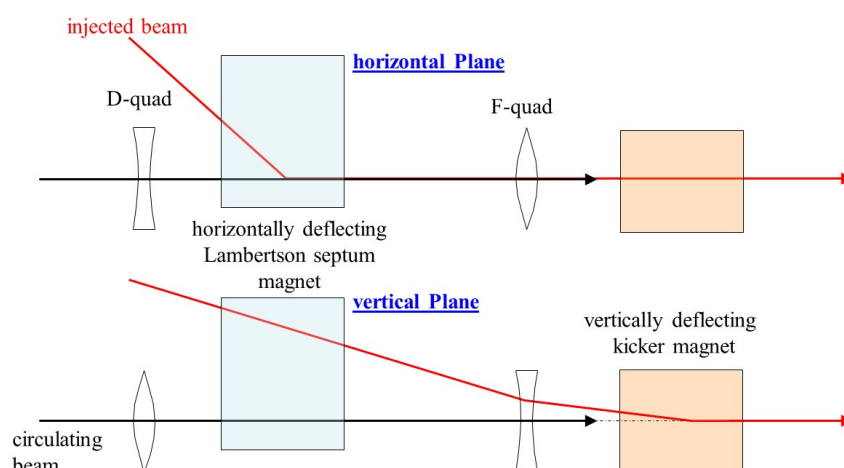
2 Single-turn (fast) injection

Figure 1 shows an example of fast single-turn injection in one plane. The injected beam passes through the homogeneous field region (gap) of the septum: the circulating beam is in the field-free region (i.e., there is space separation of the injected and circulating beams). The septum deflects the injected beam onto the closed orbit at the centre of the kicker magnet; the kicker magnet compensates the remaining angle. The septum and kicker are either side of a quadrupole (defocusing in the injection plane) which provides some of the required deflection and minimizes the required strength of the kicker magnet.
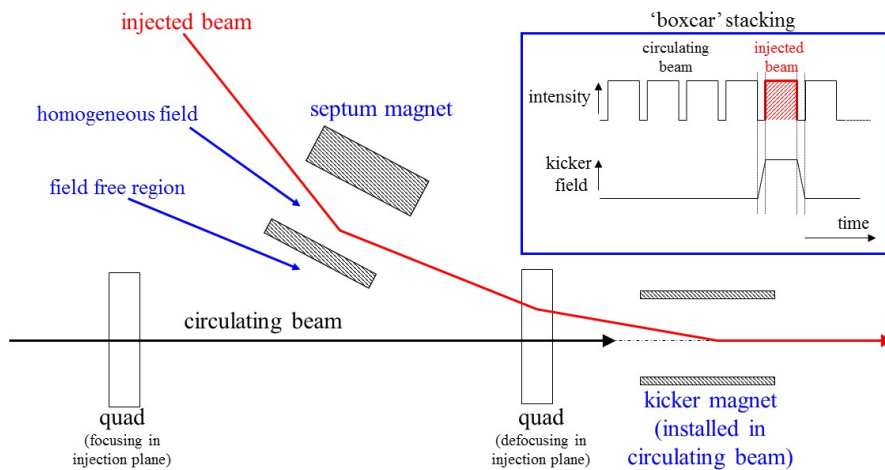
Fig. 1: Fast single-turn injection in one plane

When a kicker magnet is installed in a circular accelerator the circulating beam is typically in the aperture of the magnet. Thus the kicker field must rise from zero to full field in the time interval between the circulating beam and the start of the injected beam (Fig. 1, top right) and fall from full field to zero field in the time interval between the end of the injected beam and the subsequent circulating beam (Fig. 1, top right). The kicker system is described in more detail in section 5.

Fig. 2: Fast single-turn injection in two planes

Figure 2 shows an example of fast single-turn injection in two planes: a Lambertson septum is used for a two-plane injection scheme. The injected beam passes through the homogeneous field region of the septum: the circulating beam is in the field-free region of the septum. In the example shown in Fig. 2 the septum deflects the beam horizontally and the downstream kicker magnet deflects the beam vertically onto the closed orbit of the circulating beam. The septum and kicker are either side of an F-quadrupole (horizontally focusing but vertically defocusing) to minimize the required strength of the kicker magnet. The Lambertson septum magnet is discussed in more detail in the proceedings of this CAS, in paper *Septa*.

3   Single-turn (fast) extraction

Extraction is the process of ejecting a particle beam from an accelerator and into a transfer line or a beam dump at the appropriate time while minimizing beam loss and placing the extracted particles onto the correct trajectory, with the correct phase space parameters. Extraction usually occurs at a higher energy than injection, hence stronger elements (e.g., larger $\int B.\mathrm{d}l$) are required. At high energies many kicker and septum modules may be needed. To reduce the required strength of the kicker magnet, a closed orbit bump can be applied to bring the circulating beam near to the septum.

Figure 3 shows an example of fast single-turn extraction in one plane. The kicker magnet deflects the entire beam into the septum in a single turn [time selection (separation) of beam to be extracted]. The extracted beam passes through the homogeneous field region of the septum: the circulating beam, prior to extraction, is in the field-free region of the septum (space separation of the circulating and extracted beams). The septum deflects the entire kicked beam into the transfer line.
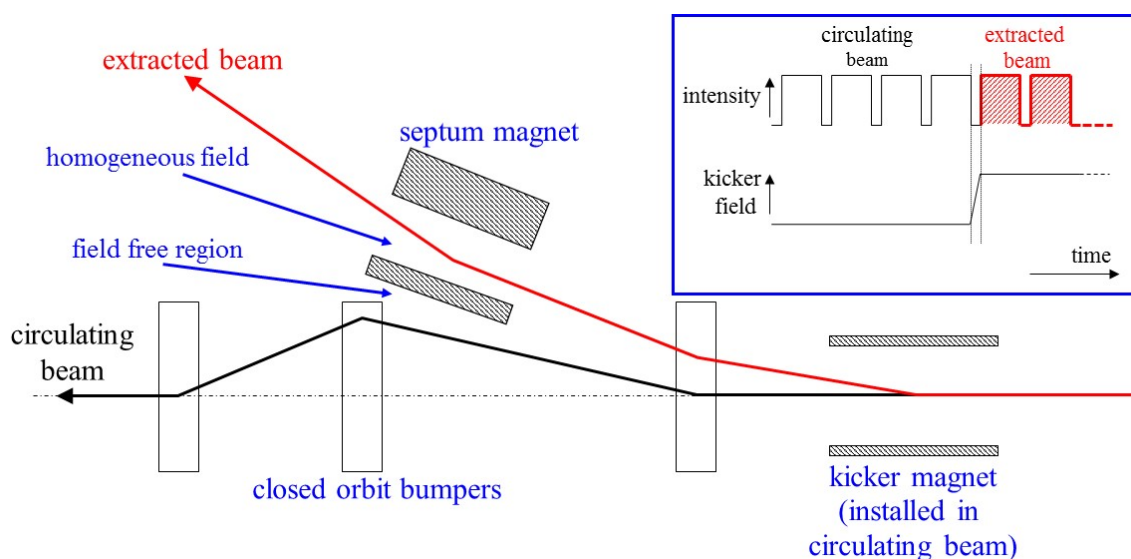
Fig. 3: Fast single-turn extraction in one plane

When a kicker magnet is installed in a circular accelerator the circulating beam is typically in the aperture of the magnet. Thus, the kicker field must rise from zero to full field in a beam-free time interval deliberately created in the circulating beam (Fig. 3, top right). The entire beam is generally extracted and hence a fast fall time is typically not required; however, sometimes, bunch-by-bunch transfers are made and then the field of the kicker magnets must have fast rise and fall times [1].

4   Deflection of beam

The force exerted on a charged particle, moving through electric and magnetic fields, is known as the Lorentz force. The Lorentz force is given by Eq. (1):

$$F = q\left[E + \left(v \times B\right)\right] \ . \tag{1}$$

In this equation:

F is the force (N);
E is the electric field (V/m);
B is the magnetic field (T);
q is the charge of the particle (C), and $q = Q \cdot e$;
e   is elementary charge ($1.602 \cdot 10^{-19}$ C);
Q is a multiple of the elementary charge (e.g., Q=1 for a proton);
v is the instantaneous velocity of the particle (m/s);
×   is the vector cross product.

Using the small angle approximation, $\tan(\theta) = \theta$, the deflection of a charged particle beam in a magnetic field is given by Eq. (2) [2]:

$$\theta_{B,x} = \left[\frac{0.2998 \cdot Q}{p}\right] \cdot \int_{z_0}^{z_1} \left|B_y\right| dz = \left[\frac{0.2998 \cdot l_{eff} \cdot Q}{p}\right] \cdot \left|B_y\right| \ . \tag{2}$$

In this equation:

B_y is the magnetic flux density in the y-direction (T);
p is the beam momentum (GeV/c);

l_{eff} is the effective length of the magnet [usually different from the mechanical length, due to fringe fields at the ends of the magnet] (m);

$\theta_{\text{B},x}$ is the deflection angle, in the x-direction, due to magnetic field B_y (radians).

Using the small angle approximation $\tan(\theta) = \theta$, the deflection of a charged particle beam in an electric field is given by Eq. (3) [2]:

$$\theta_{E,x} = \left[\frac{Q}{(p \cdot 10^9) \cdot \beta} \cdot \int_{z_0}^{z_1} |E_x| dz \right] = \left[\frac{|V| \cdot l_{eff} \cdot Q}{d \cdot (p \cdot 10^9) \cdot \beta} \right] . \tag{3}$$

In this equation:

V is the potential difference between plates (V);
d is the separation of the plates (m);
E_x is the electric field in the x-direction (V/m);
β is a unit-less quantity that specifies the fraction of the speed of light at which the particles travel (v/c);
$\theta_{E,x}$ is the deflection angle, in the x-direction, due to electric field E_x (radians).

5   Kicker system

5.1   Overview

Figure 4 shows a simplified schematic of a kicker system. The main sub-systems ('components') of a kicker system are:

– pulse forming line (PFL) (coaxial cable) or pulse forming network (PFN) (lumped elements);
– kicker magnet;
– fast, high power, switch(es);
– resonant charging power supply (RCPS);
– transmission line(s) [coaxial cable(s)];
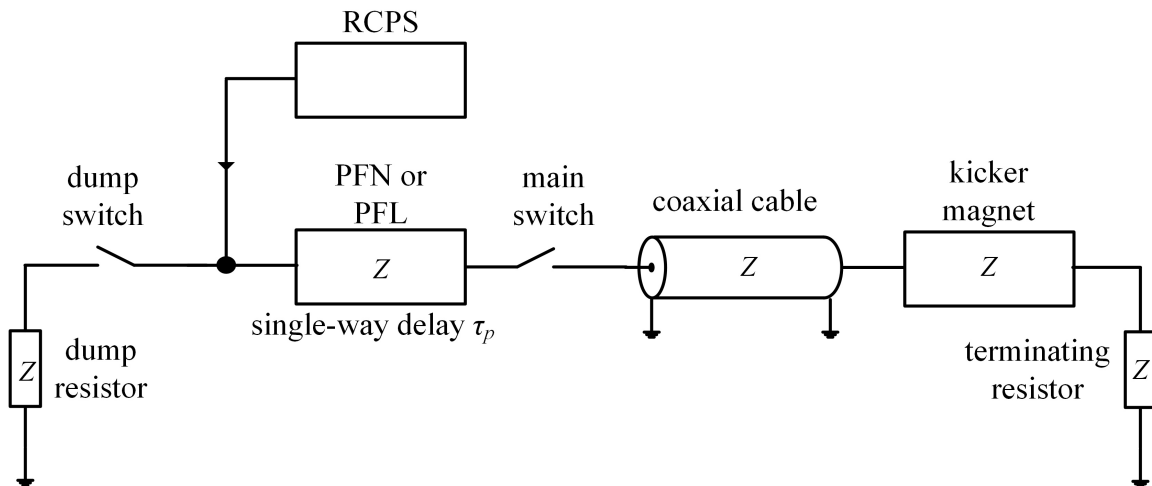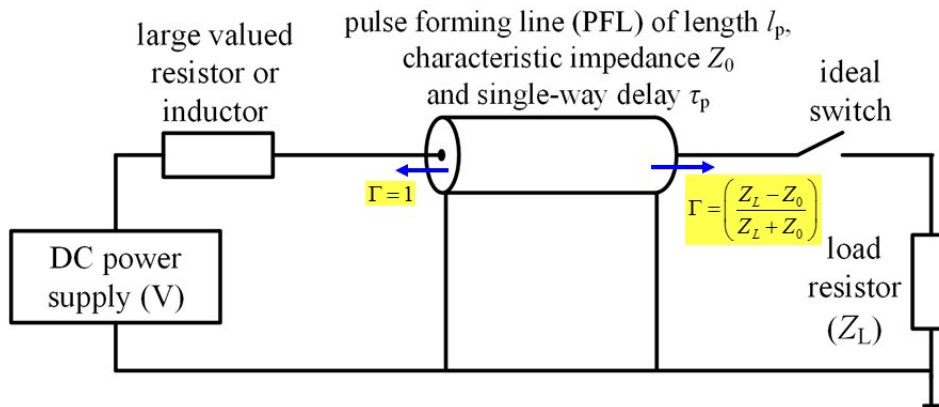– resistive terminators.

Fig. 4: Simplified schematic of a kicker system

5.2 Pulse forming circuit: general case

Figure 5 shows a simplified schematic of a pulse-forming circuit: the switch is initially open and the coaxial cable (PFL) is pre-charged, through the large valued resistor or inductor, to a voltage V.

Fig. 5: Simplified schematic of a pulse-forming circuit

At time $t = 0$, when the ideal switch closes, the load voltage is given by Eq. (4):

$$V_L = \left(\frac{Z_L}{Z_0 + Z_L} \right) V = \alpha V \ , \tag{4}$$

In this equation:

$$\alpha = \left(\frac{Z_L}{Z_0 + Z_L} \right);$$

V_L	is the load voltage (V);
V	is the initial voltage to which the PFL is charged (V);
Z_L	is the load impedance (Ω);
Z_0	is the characteristic impedance of the PFL (Ω).

Figure 6 shows a lattice diagram for the general case (impedances not necessarily matched) for the voltage on the PFL. At time $t = 0$, when the switch closes, a voltage pulse of '$(\alpha - 1)V$' propagates from the load end of the PFL towards the charging end. At the charging end of the PFL the reflection coefficient (Γ) is +1 and hence a voltage of '$(\alpha - 1)V$' is reflected back towards the load end of the PFL. At the load end of the PFL the reflection coefficient is given by Eq. (5):

$$\Gamma = \left(\frac{Z_L - Z_0}{Z_L + Z_0} \right) = \beta \ , \tag{5}$$

and hence a voltage of '$\beta(\alpha - 1)V$' is reflected back towards the charging end of the PFL, etc.
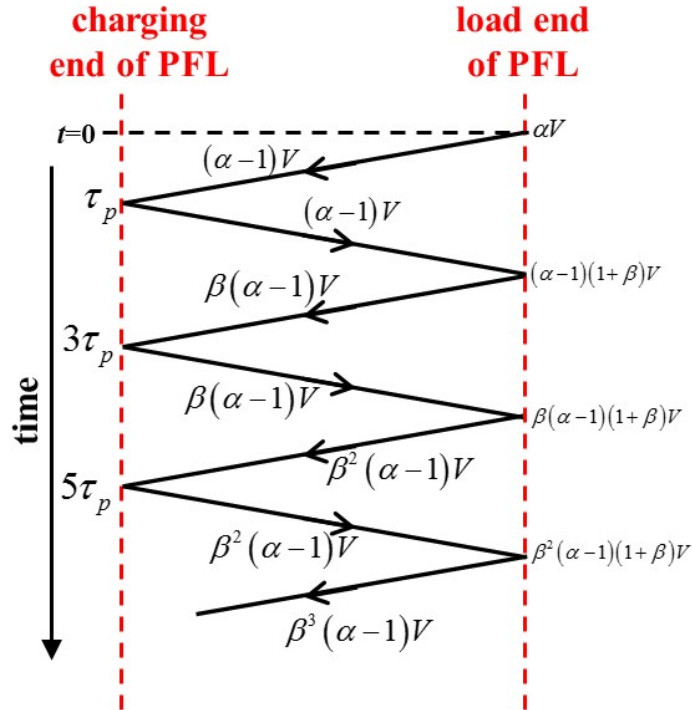
Fig. 6: Lattice diagram for the pulse forming circuit of Fig. 5 (general case)

Impedances need to be matched to avoid reflections, i.e., from Eq. (5), when $Z_L = Z_0 \rightarrow \beta = 0$. When the impedances are matched:

- PFN/PFL is charged to a voltage V by the RCPS;

- the main switch (MS) closes (Fig. 4) and, for a matched system, a pulse of magnitude $V/2$ is launched, through the coaxial cable, towards the kicker magnet. A voltage pulse of magnitude $-V/2$ propagates from the load end of the PFN/PFL towards the charging end;

- once the flat top of the current pulse reaches the (matched) terminating resistor (TMR), full field has been established in the kicker magnet (section 5.3.3);

- the duration of the pulse in the magnet can be controlled in length, between 0 and $2\tau_p$, by adjusting the timing of the dump switch (DS) (Fig. 4) relative to the MS.

Note: if the magnet termination is a short circuit, the magnet current is doubled but the 'fill time' of the magnet is doubled too (section 5.3.6). In this case, the DS may be an inverse diode: the inverse diode 'automatically' conducts when the PFN voltage reverses, at the charging end of the PFL/PFN, but there is no control over the pulse length in the magnet.

5.3 Kicker magnet

5.3.1 History

Figure 7 shows a 1970s 'plunging' kicker magnet, which was hydraulically operated [3]: the aperture was too small for the kicker to be in the beam line during circulating beam. Developments leading to higher current pulses permitted larger apertures: kicker magnets developed later at CERN were not hydraulically operated.
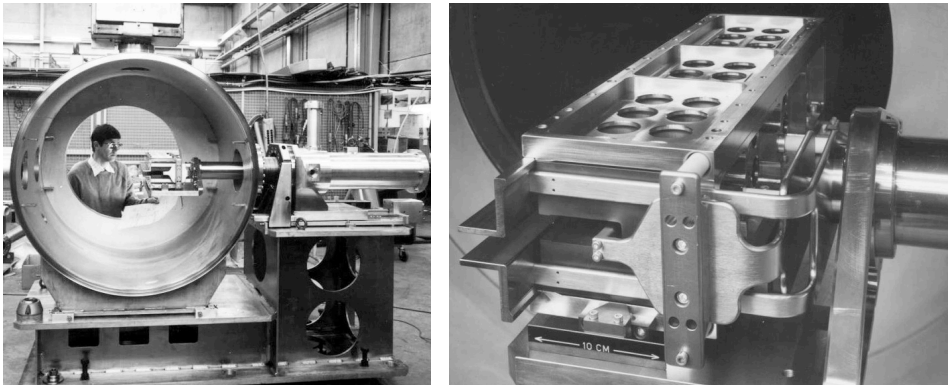
Fig. 7: A 1970s plunging kicker magnet for ejection from the CERN Antiproton Accumulator (AA)

5.3.2 *Overview*

Figure 8 shows a cross-section of a typical C-core kicker magnet with the return conductor closing the aperture. Fast kicker magnets generally have a ferrite yoke and are transmission line type magnets with a rectangular-shaped aperture of dimensions H_{ap} by V_{ap} (Fig. 8).

Assuming a high relative permeability for the yoke, the flux density in the aperture (B_y) of the kicker is given by Eq. (6):

$$B_y \cong \mu_0 \left(\frac{N \cdot I}{V_{ap}} \right) , \qquad (6)$$

where:

μ_0 is permeability of free space ($4\pi \times 10^{-7}$ H/m);

N is the number of turns (usually 1 for a kicker magnet);

I is magnet current (A);

V_{ap} is the distance between the inner edges of the 'legs' of the ferrite (m).
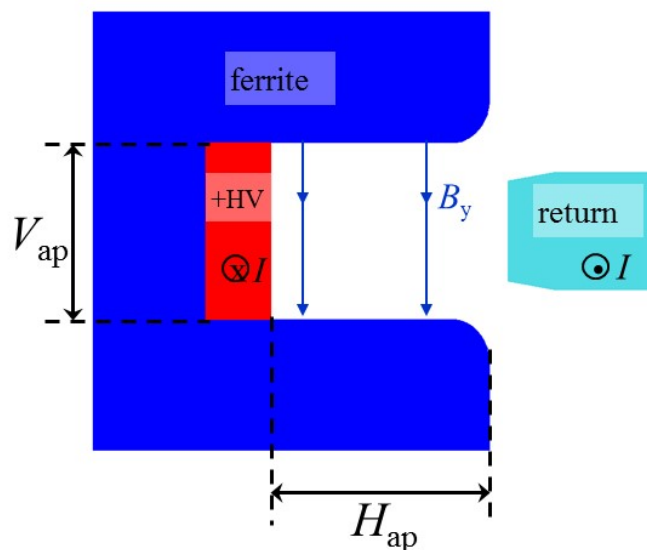

Fig. 8: Cross-section of a typical C-core kicker magnet

The skin effect and proximity effect result in current flow on the inside surface of both the high voltage (HV) and return conductors. Hence, assuming a high relative permeability for the yoke, inductance is given by Eq. (7):

$$L_{m/m} \cong \mu_0 \left(\frac{N^2 \cdot H_{ap}}{V_{ap}} \right) , \tag{7}$$

In this equation:

H_{ap} is the distance between the inner edge of the HV conductor and the end of the leg of the magnetic material (m);

$L_{m/m}$ is inductance per metre length of the kicker magnet (H/m).

Since kicker magnets generally need to be fast, they usually have a single-turn coil ($N = 1$): multi-turn coils are used only for slower, lumped-inductance, kicker magnets.

The deflections of a charged particle in a magnetic field and an electric field are given by Eq. (2) and Eq. (3), respectively. For a transmission-line kicker magnet, where ferrite C-cores are sandwiched between HV capacitance plates (see section 5.3.3.2), end effects result in an effective length of each end cell approximately $\left(V_{ap}/4 \right)$ greater than its physical length [4]. Thus the effective length of the kicker magnet is increased by an amount approximately equal to $\left(V_{ap}/2 \right)$, in comparison to the physical length of the aperture.

5.3.3 *Design options for kicker magnets*

Design options for kicker magnets include the following [3].
-   Type: 'lumped inductance' or 'transmission line' (with specific characteristic impedance (Z))
-   Machine vacuum: install in or external to machine vacuum
-   Aperture: window frame, closed C-core or open C-core
-   Termination: matched impedance or short circuited

5.3.3.1 Lumped-inductance kicker magnet

Although a lumped-type magnet has a simple structure, in many cases it cannot be applied to a fast kicker system because of its impedance mismatch and its slow response [5]. The lumped-inductance kicker is generally useable only when a rise time above a few hundreds of nanoseconds is required. The lumped-inductance kicker either has a resistor in series with the kicker magnet input or else the resistor is omitted. In both cases, the kicker magnet only sees voltage during pulse rise and fall: the magnet voltage during field fall time is the opposite polarity compared too field rise. With a short-circuit termination, magnet current is doubled for a given PFN/PFL voltage and system characteristic impedance.

For a magnet inductance L_m with a resistor in series with its input, combined with a pulse generator of impedance Z, the rise of the magnet current is exponential with a time constant t_{cl} given by Eq. (8):

$$t_{cl} = \left(\frac{L_m}{Z + R} \right) . \tag{8}$$

The 5% to 95% rise time of the current is as long as three time constants. To help to overcome the long rise time, a capacitor can be connected in parallel with, at the entrance of, the lumped-inductance magnet, but this can provoke some overshoot.

5.3.3.2   Transmission-line kicker magnet

To overcome the long rise time, the first transmission-line kicker magnet was developed at CERN in the early 1960s [5]. A transmission-line magnet consists of few to many 'cells' to approximate a broadband coaxial cable (Fig. 9). Ferrite C-cores are sandwiched between HV capacitance plates: plates connected to ground are interleaved between the HV plates. The HV and ground plates form a capacitor to ground (Fig. 9). One C-core, together with its ground and HV capacitance plates, is termed a cell. Each cell conceptually begins and ends in the middle of the HV capacitance plates. The 'fill time' of the magnet (τ_m) is the delay required for the pulse to travel either one way, if the magnet is terminated in its characteristic impedance, or two ways, if the magnet is terminated in a short circuit, through the 'n' magnet cells.
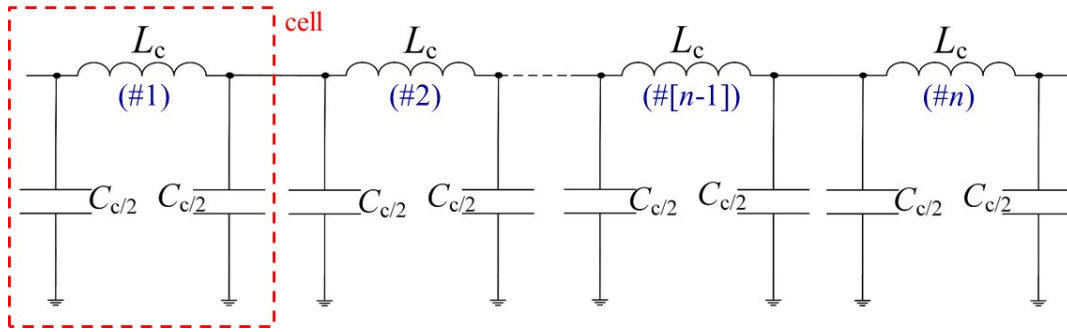
Fig. 9: Simplified equivalent electric circuit of a transmission-line kicker magnet

The characteristic impedance (Z) of the kicker magnet, which is matched to the impedance of the generator to minimize reflections [6, 7] (see section 5.2), is given by Eq. (9):

$$Z = \sqrt{\frac{L_c}{C_c}} \ , \qquad (9)$$

In this equation:

L_c is the inductance of a cell of the kicker magnet (H);
C_c is the capacitance of a cell of the kicker magnet (F).

The single-way delay of the kicker magnet is given by Eq. (10):

$$\tau_m = n\sqrt{L_c \cdot C_c} = n\left(\frac{L_c}{Z}\right) = \left(\frac{L_m}{Z}\right) \ , \qquad (10)$$

In this equation:

neglecting end effects, $L_m = n(L_c)$,

L_m is the total inductance of the kicker magnet (H).

For a kicker magnet terminated with a matched resistor, field rise time begins with the start of the rising edge of the voltage pulse at the entrance of the kicker magnet and finishes with the end of the rising edge of the pulse at the exit of the magnet. Flux is given by the time integral of the difference between the voltage at the magnet entrance and exit [Eq. (11)]:

$$\Phi = \int \left(V_{in}(t) - V_{out}(t)\right)\mathrm{dt} \ , \qquad (11)$$

In this equation:

Φ is flux (V·s);
$V_{in}(t)$ is the voltage at the entrance to the kicker magnet (V);
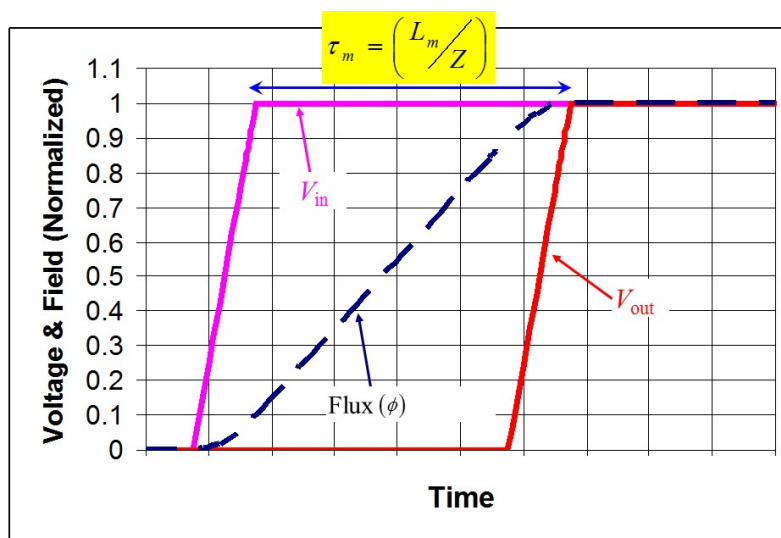$V_{out}(t)$ is the voltage at the exit of the kicker magnet (V).

Fig. 10: Flux in an 'ideal' transmission-line kicker magnet

The flux builds up until the end of the voltage rise at the exit of the kicker magnet (Fig. 10): thus, for an ideal transmission-line kicker magnet terminated in its characteristic impedance, flux rise time is given by the sum of the voltage rise time and the single-way delay of the magnet. The single-way delay, in this case, corresponds to the magnet fill time. Therefore it is important that the pulse does not degrade while travelling through the kicker magnet. Hence, the magnet cut-off frequency is a key parameter, especially with field rise times below ~100 ns. Cut-off frequency (f_c) depends on series inductance (L_{cs}) associated with the cell capacitor (C_c) [3]:

$$f_c = \frac{1}{\pi \cdot \sqrt{(L_c + 4L_{cs}) \cdot C_c}} = \frac{Z}{\pi \cdot \sqrt{(L_c + 4L_{cs}) \cdot L_c}} \quad . \tag{12}$$

Thus, to achieve a high cut-off frequency, L_{cs} should be kept as low as possible and the cell length small, i.e., low cell inductance and cell capacitance. However, cells cannot be too short because an adequate distance is required between the HV and ground capacitance plates to avoid voltage breakdown. In addition, many very short cells would significantly increase the cost and complexity of the kicker magnet.

Figure 11 shows the results of a low-voltage measurement on each of the HV capacitance plates of a transmission-line kicker magnet. The fast rise time of the input voltage pulse, used for the measurements, contains frequency components above the cut-off frequency of the cells. Thus there is an increase in the rise time of the voltage pulse between the entrance HV capacitance plate and the second HV capacitance plate; in addition there is significant ripple on the pulses.
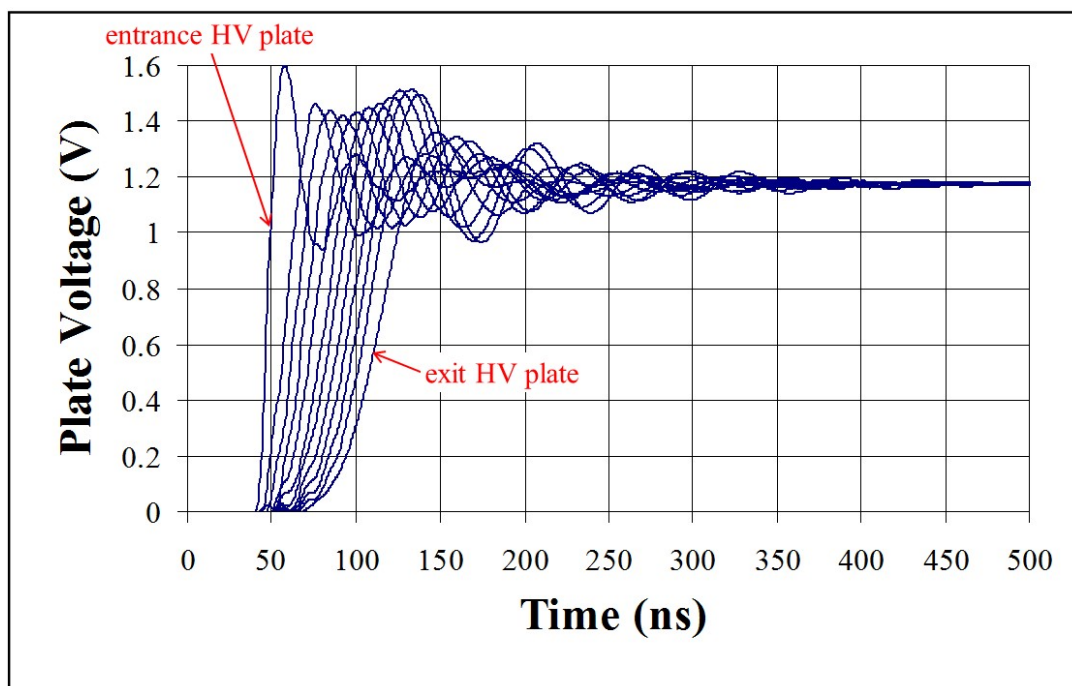
Fig. 11: Low voltage measurement on each of twelve HV capacitance plates of an eleven-cell transmission-line kicker magnet.

The choice of the characteristic impedance, for a transmission-line magnet, depends upon the required field rise/fall time and the available length for the kicker magnet. In general the highest impedance, up to the impedance of commercially available coaxial cable (50 Ω), is used while still respecting the available length for the kicker magnet and chosen level of PFN voltage [3]. The higher the characteristic impedance, the higher the magnet cut-off frequency (Eq. (12)): a high cut-off frequency reduces the field ripple.

A vacuum dielectric transmission-line kicker magnet can require a very large area of metal plates to form the capacitance, especially for a low-impedance system. Since the minimum separation of the capacitor plates is determined by practical considerations, such as voltage breakdown and cost, the capacitance is determined by the area of the plates; however, Eq. 9 shows that the capacitance (area) must increase by a factor of 4 for a decrease in impedance by a factor of 2 (neglecting edge effects). It has been shown that it is feasible to design a 'hybrid' kicker magnet, which is an effective transmission kicker magnet with a fast rise time, using only 3 to 5 large cells [8], but which requires large capacitance values. However, it is impractical for lower impedance magnets or for magnets with larger cell inductances to use vacuum dielectric capacitors. Hence, with the space limitation at many accelerator facilities, the application of higher permittivity dielectric capacitor media is necessary [7, 9].

5.3.4   *Machine vacuum*

The minimum-sized aperture for a kicker magnet can be achieved if the magnet is in vacuum: if the magnet is outside vacuum, a chamber must be inserted in the kicker aperture, thus increasing the dimensions of the aperture. The minimum value of both H_{ap} and V_{ap} (Fig. 8) are determined by beam parameters. Equation (7) shows that magnet inductance is proportional to H_{ap} and inversely proportional to V_{ap}. However, if V_{ap} is increased, although the magnet inductance is reduced, this is at the expense of increased current to obtain a given flux density (Eq. 6): increased current also requires, for given impedance, increased PFN/PFL voltage and thus increased insulation requirements.

Advantages of putting a transmission-line kicker magnet in the machine vacuum are the following.

–   Aperture dimensions are minimized, therefore the number of magnets and/or voltage and current are minimized for a given ∫B.dl and rise time.

–   Machine vacuum is a reliable dielectric (70 kV/cm is OK [3]) and generally 'recovers' after a flashover, whereas a solid dielectric, outside vacuum, may not recover.

Disadvantages of putting a transmission-line kicker magnet in the machine vacuum are the following.

–   The kicker magnet is costly and time consuming to construct (all parts must be appropriately cleaned and handled, a vacuum tank is required, and suitable pumps are needed. If the kicker magnet must be baked out, to achieve the required vacuum level, the design may need to allow for thermal expansion during bake out, etc.).

–   In the event of failure of something inside the vacuum tank, the vacuum must be broken to repair the fault. Afterwards, pumping, bake out (if appropriate), and HV conditioning are required—a time-consuming process.

The beam-coupling impedance may be an issue irrespective of whether the magnet is in vacuum. Hence a beam screen (see section 5.5) in the kicker aperture, may be required: this will require an increase in aperture dimensions in any case.

5.3.5   *Kicker magnet aperture*

Normally a magnetic circuit is used which contains magnetic material [3, 5]: without magnetic material the effective value of V_{ap} (Fig. 8) is greatly increased, therefore requiring more current to achieve the required field (Eq. 6). In addition, magnetic material improves field uniformity. Nickel-zinc (NiZn) ferrite, with initial $\mu_r \approx 1000$, is typically used [1, 3]. If the ferrite is in machine vacuum (section 5.3.4) the out-gassing properties must be acceptable: in addition, the density of the ferrite must be such that its water absorbent characteristics are not too high and no undesirable lubricants must be used during the grinding process [1]. At CERN, 8C11 ferrite (Ferroxcube) and CMD5005 ferrite (National Magnetics Group, Inc.) are currently used, although other types of ferrite are under consideration. The 8C11 and CMD5005 ferrites have the following properties:

–   field rise can track current rise to within ~1 ns [3];
–   low remnant field;
–   low out-gassing rate, after bake out.

Figure 12 shows a full-aperture C-core magnet (Left Hand Side (LHS)) and a window-frame magnet ((Right Hand Side (RHS)). The C-core magnet shown in Fig. 8 has its aperture closed by the return conductor. The C-core magnet on the LHS of Fig. 12 has the return conductor behind the yoke: this is for beam gymnastic reasons and has the effect of increasing the effective width ($H_{ap(eff)}$) of the magnet aperture, of given dimensions, from H_{ap} to a value given approximately by Eq. (13) [10, 11]:

$$H_{ap(eff)} \approx \left(H_{ap} + V_{ap}/2 \right) . \tag{13}$$

Similarly, the inductance of a cell of the full-aperture kicker magnet is increased by a factor of $\left(H_{ap(eff)}/H_{ap} \right)$ with respect to the return conductor closing the aperture of the kicker magnet.
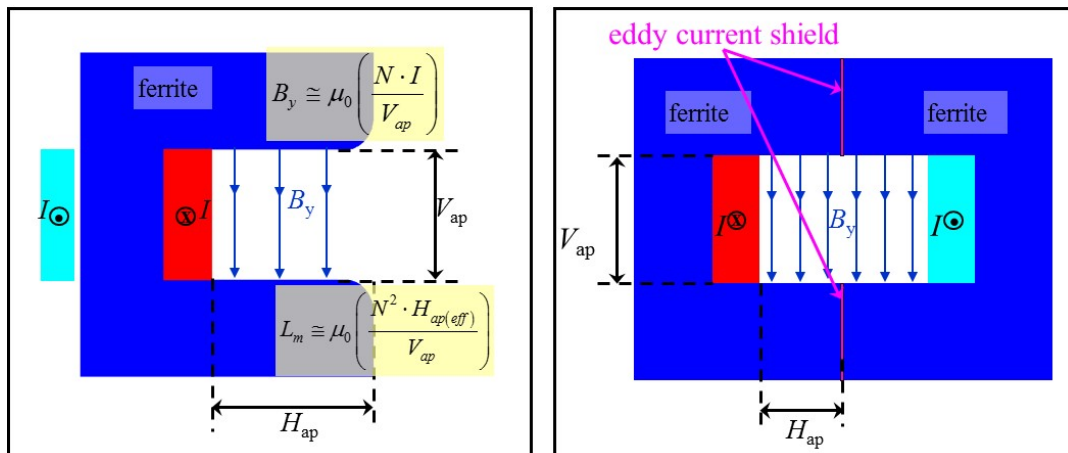
Fig. 12: Full-aperture C-core magnet (LHS) and window frame magnet (RHS)

To reduce magnet fill time by a factor of two, FNAL and KEK use a window-frame topology (RHS of Fig. 12): it can be considered as two symmetrical C-magnets energized independently. However, the window-frame magnet requires two generators to achieve the reduced magnet fill time [5]. It is necessary to include eddy current 'shields' between the two ferrite C-cores to reduce beam-coupling impedance (see section 5.5).

C-core kicker magnets are generally used at CERN.

5.3.6   *Kicker magnet termination*

When space along the beam line is at a premium, a short-circuit termination has the advantage over a matched resistive termination of doubling current and hence field (for a given system impedance) [3]: in addition, a short-circuit termination reduces the time during which the kicker magnet is exposed to high voltage. However, disadvantages include:

-    for a given magnet length and impedance, fill time of the kicker magnet is doubled: to establish full field in the magnet, the current/voltage pulse must propagate from the input to the output of the magnet and then reflect back to the input;

-    the kicker magnet experiences voltage of both polarities: one polarity during field rise and the opposite polarity during field fall (the incident voltage wavefront is inverted at the short-circuit termination [reflection coefficient is −1]);

-    if the DS is used to control pulse length it must be bidirectional (unidirectional DS, acting as an inverse diode, is suitable for a fixed length pulse);

-    beam-coupling impedance can be influenced (see section 5.5).

5.4   **Kicker magnet design tools**

Circuit simulation and finite element codes greatly assist the goal of obtaining high performance kicker systems. Simulation of circuits which include almost all known parasitic elements and non-linearities is now possible [5].

Two- and three-dimensional (3D) finite element codes now include AC and transient analysis with eddy currents. These tools are used for kicker magnet design to predict magnetic field, cell inductance, electric field [13–15], and capacitance. In order to obtain realistic predictions for inductance and magnetic field distribution, in the aperture of the kicker magnet, it is necessary that the skin effect and proximity effect, in the HV and 'ground' (return) conductors (Fig. 13), be properly accounted for: this requires an AC or transient analysis to be carried out. Codes such as *Opera2D* and *Opera3D* [16]

are also used to study the shape of the ferrite and conductors and thus optimize the field homogeneity [14, 15]; the current distribution is calculated by the code. The LHS of Fig. 13 shows a transmission-line kicker magnet used to deflect the beam horizontally. The magnet was modelled using *Opera2D* to predict the magnetic and electric field distribution. The predictions were post-processed and the total deflection calculated; the RHS of Fig. 13 shows a plot of deflection uniformity for the optimized geometry of ferrite and return conductor [14, 15].

The penetration of the pulsed field through a beam screen (section 5.5), in a magnet aperture, can also be accurately calculated and the frequency dependence of magnet inductance, due to eddy currents in the screen, predicted [17]. An equivalent circuit can then be fitted to the resulting predictions to account for the frequency dependence in an analogue circuit simulation [18].

An AC analysis can also be used to predict the frequency dependence of both inductance and resistance, i.e., skin effect and proximity effect, due to eddy currents in PFN coils [18, 19] (see section 5.8). An equivalent circuit can be fitted to the resulting predictions to account for the frequency dependence in an analogue circuit simulation. The electric circuit models can also include displacement current during turn on of a multi-gap thyratron (section 5.9.1).
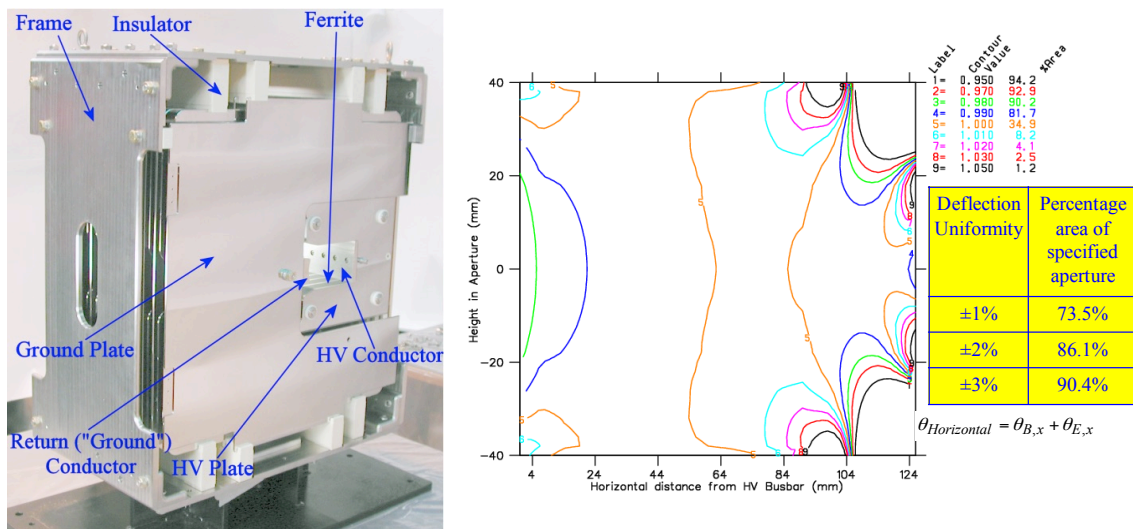

Fig. 13: Transmission-line kicker magnet and corresponding deflection uniformity plot

In addition, capacitance to ground of a HV plate, in a kicker magnet, is influenced by insulators and nearby ground planes such as the:
- ground plate;
- magnet frame;
- return conductor.

Boundary element software such as *Coulomb*, a 3D code from Integrated Engineering Software [20], can be used to accurately predict the capacitance of a cell of a kicker magnet. The predictions resulting from *Coulomb* have been carefully checked against measurements and found to be in good agreement [4].

Thermal analysis packages such as *ANSYS* [21] are used to assess transient and steady-state temperatures of, for example, the yoke of a kicker magnet (section 5.6). *ANSYS* can also be used to assess mechanical stress on magnet components during rapid heating or cooling.

Powerful simulations tools such as *CST Particle Studio* [22], which can model frequency-dependent permittivity and permeability (e.g., of ferrite), can be used to predict the beam-coupling impedance for complex structures such as kicker magnets, and determine beam-induced power

deposition in volumes of the structure (section 5.5). The high frequency structure simulator (*HFSS*) [21] can be used for beam-coupling impedance and field homogeneity simulations (section 5.10).

5.5   Beam-coupling impedance

High-intensity accelerators are very sensitive to longitudinal and transverse beam-coupling impedance. Kicker magnets, with their ferrite yoke, can result in considerable beam-coupling impedance [23−27], and can be one of the dominant sources of impedance [28], which can limit the intensity reach of an accelerator. The real component of the longitudinal beam-coupling impedance, together with the beam spectrum, results in beam induced power deposition in the ferrite yoke [23−27, 29−31], sometimes heating the yoke beyond the Curie temperature. If the yoke exceeds its Curie temperature, it will temporarily lose its magnetic properties: as a result, beam could be miskicked. Hence, it would be necessary to allow the yoke to cool below its Curie temperature before using the system to inject or extract beam: because of long thermal time constants this could require several hours [32]. In extreme cases beam-induced power can affect the generator as well [33].

There are formulae for estimating the beam-coupling impedances of kicker magnets e.g., Refs. [34−37]. Nevertheless, *CST Particle Studio* [22] is an important software tool for predicting beam-coupling impedance, especially for complex geometries and dispersive materials, understanding the source of both broadband impedance and impedance resonances, and optimizing a design [25−27]. Beam-coupling impedance measurements can be made using a coaxial wire method, which is also an invaluable tool [12, 23]. Standard wire measurement techniques are described in [38]. Wire measurements rely on the fact that an ultra-relativistic beam has a very similar electromagnetic field distribution to that of a transverse electromagnetic (TEM) line [23]. Generally speaking, the wire diameter should be as small as possible to get a high line impedance [23].

Some beam-coupling impedance resonances are attributable to the image path of the beam not being continuous, for example, a gap between the end of the kicker magnet and the vacuum tank. In this case, these geometrical resonances can be eliminated by inserting transition pieces inside the tank to electrically connect the tank flange to the kicker magnet at each end [29, 42−44]. When several kicker magnets are installed in a common tank, the transition between magnets is carried out in a similar way [5].

Longitudinal beam-coupling impedance of the ferrite yoke of a kicker magnet is reduced by providing a beam screen in the magnet aperture [12, 17, 23−27, 30, 39−41]. The metallic parts of the screen conducts the beam image current and hence the electromagnetic fields penetrating the ferrite are reduced in magnitude but, at the same time, the screen must not significantly attenuate the pulsed field. An alumina chamber is often placed in the aperture of a kicker magnet. A thin metallic coating is frequently applied to the inner surface of the alumina chamber to both screen the kicker magnet yoke from the beam [e.g., 45−48], and also to prevent build-up of static charge on the chamber [47]. It is important that the metallization does not unduly degrade field rise/fall times or the flat top of the field pulse in the kicker magnets. This is of particular concern for kicker magnets that have a fast field rise and/or fall time. The impact of the metallization on the transient field response can be studied using finite element method (FEM) simulations [48]. For lumped element kicker magnets, analytic formulae also allow a rapid evaluation of the influence of the metallic coating upon field rise and fall. The time constant for the metallized coating, obtained from these formulae, can then be incorporated in a *PSpice* model of the kicker system so that arbitrary excitation waveforms can be considered and the system optimized for the required magnetic field rise and fall times [48].

The LHS of Fig. 14 shows longitudinal beam-coupling impedance reduction techniques for the MKE kickers [23], used for extraction from the CERN super proton synchrotron (SPS) ring. Two sets of silver fingers are printed directly on the ferrite, by serigraphy: each set of fingers is connected to a high-voltage plate. The serigraphy fingers cannot be continuous between the two high-voltage plates, as this would create eddy-current loops and hence can significantly increase field rise time. The spacing

between the two sets of fingers, for the MKE, is 20 mm: this spacing is chosen for high-voltage reasons. The length of the MKE ferrite block is 230 mm. The serigraphy does not reduce the available aperture.
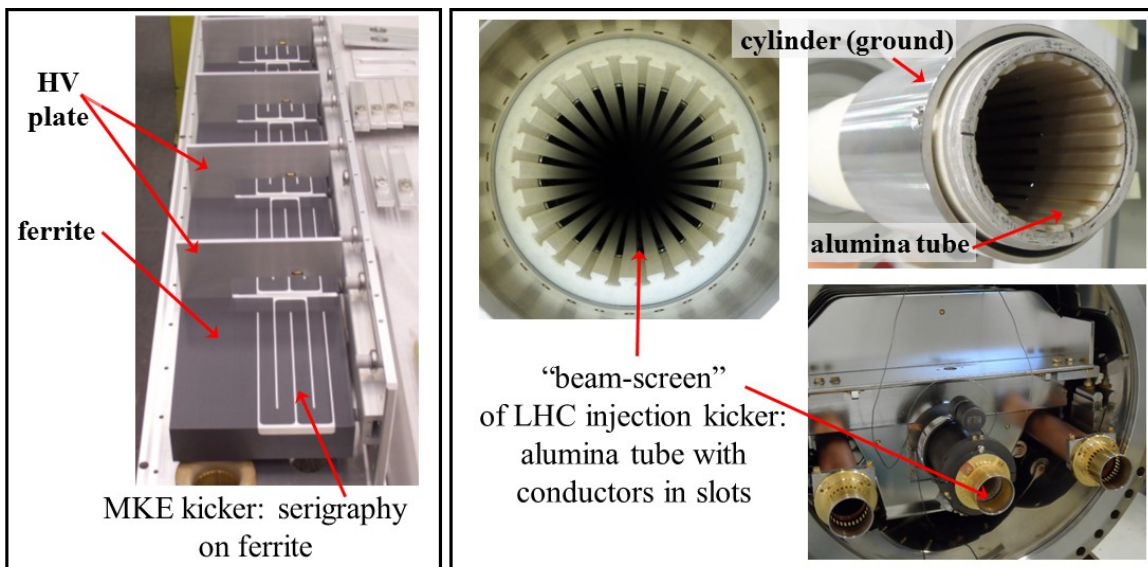

Fig. 14: Beam-coupling impedance reduction techniques for the MKE (LHS) and MKI (RHS) kickers

Figure 15 shows longitudinal beam-coupling impedance for several systems; unless mentioned otherwise, the impedance is derived from measurements: the serigraphy results in a strong reduction of the real part of the longitudinal beam-coupling impedance over a broad frequency range. At the same time the serigraphy introduces a quarter-wavelength resonance [25]: the resonant frequency is dependent upon properties of the ferrite (permittivity and permeability [which are frequency dependent]), and the length of the serigraphy fingers. This resonance is clearly visible in Fig. 15, at approximately 50 MHz, in the measured impedance of the serigraphed MKE-L magnet: the length of the serigraphy fingers, for this case, is 200 mm. Hence, to limit beam-induced power deposition, the length of the serigraphy fingers should be optimized to avoid a high-impedance resonance close to the frequency of a beam harmonic [25]. Furthermore, care must be taken to ensure that an impedance resonance does not result in beam instabilities.

The thickness of the serigraphy must be sufficient to achieve the objective of adequately reducing the longitudinal beam-coupling impedance but thin enough such that field rise time is not significantly increased [49]. Recent *CST* simulations show that serigraphed fingers would not be effective at reducing beam-induced power deposition when applied to individual cells of a kicker magnet that has relatively short cells: for example, the CERN SPS injection kickers (MKP) [27] the MKP-L ferrite length is only 26 mm per cell: approximately 1/9th of the MKE ferrite length per cell. With short cell length, to achieve sufficient coupling between the two sets of fingers, the serigraphy must extend over a significant portion of the length of the yoke. Thus, the serigraphy must cross the MKP HV plates, which sandwich the ferrite cores. Hence, insulation is required between the magnet and the serigraphy: for the MKP it is expected that the serigraphy would be applied to alumina plates [27, 50].
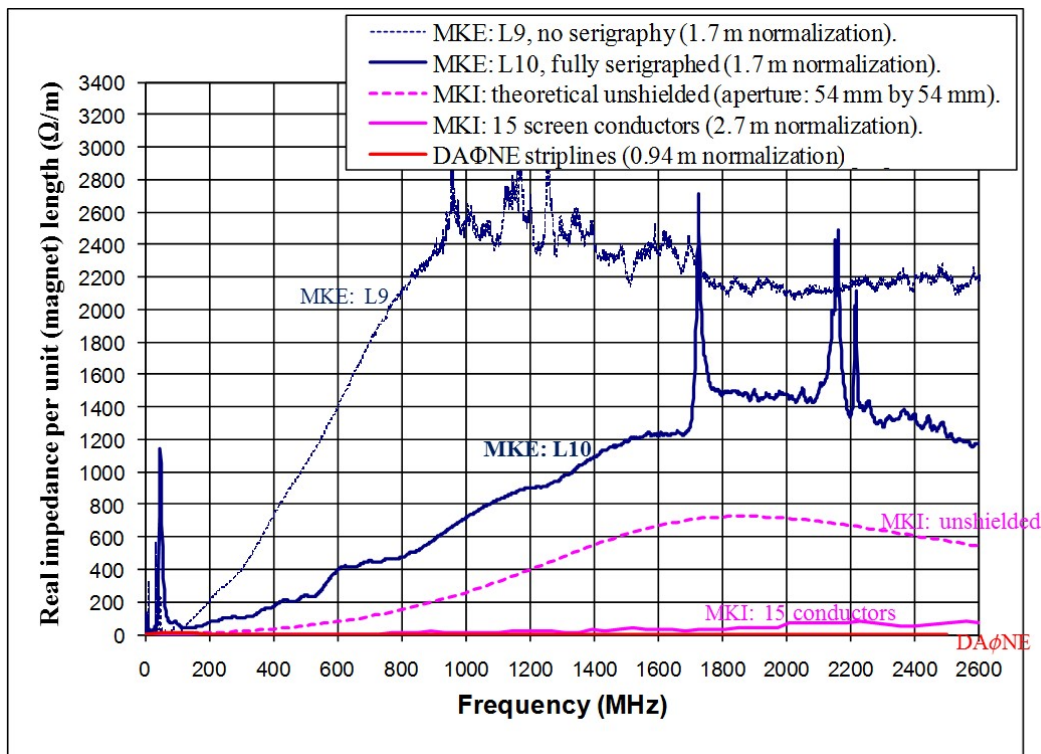
Fig. 15: Real component of longitudinal beam-coupling impedance for several systems, terminated in their characteristic impedance.

Longitudinal beam-coupling impedance measurements on the SPS extraction kicker magnets show that the high impedance resonance at ~50 MHz (Fig. 15) is only present with serigraphy [12]. Detailed measurements show that this resonance is also influenced by the external circuit on the output of the magnet (resistor termination or short circuit): for an SPS MKE, with the pulse input end open circuit, terminating the kicker magnet output in a short circuit, rather than its characteristic impedance, results in an increase in the expected beam induced power deposition by almost 10%.

Longitudinal beam-coupling impedance measurements, on a kicker magnet terminated in a short circuit, with coaxial cables on its input, have been carried out [44]: when the MS thyratron is in the off state (Fig. 4), the transmission cables between the MS thyratron and the input to the kicker magnet are effectively terminated in an open circuit at the MS end. The measurements show that below ~45 MHz impedance resonances were produced by electrical resonant modes of the kicker system: the resonances correspond to that of a half-wavelength resonator, i.e., with one end open circuit and the other short circuit. Above 45 MHz there is not strong coupling to the electrical circuit of the kicker system hence, above 45 MHz, the longitudinal beam-coupling impedance spectrum did not depend strongly upon the electrical termination on the output of the magnet [44]. Beam based measurements of kicker impedances also show that a kicker magnet with coaxial cables on its input and terminated in a short circuit exhibit impedance resonances, many of which are supressed by a resistive termination [51]. Similarly, measurements carried out with the output of the magnet terminated in its characteristic impedance show that the presence or absence of coaxial cable on the input of the magnet, terminated remotely in an open circuit, has a small, but measurable, effect upon beam-coupling impedance.

A saturating inductor can be placed at the electrical input to the kicker magnet to reduce the effect of displacement current, during turn on of a multi-gap thyratron, upon field rise time (section 5.9.1). Longitudinal beam-coupling impedance measurements have been carried out, on a kicker magnet terminated in a short circuit, to assess the influence of the saturating inductor: resonances due to the input transmission cables are effectively eliminated by the presence of the saturating inductor [44]. In

addition, a series resistor−capacitor (known as a speed-up network), connected from the kicker magnet side of the saturating reactor to ground, can be used to reduce the magnitude of the remaining impedance resonances [44].

The RHS of Fig. 14 shows longitudinal beam-coupling impedance reduction techniques implemented for the MKI kickers, used for injection into the CERN large hadron collider (LHC) rings. A 3 m long alumina tube is manufactured with 24 slots on its inside diameter [17]; however, this tube results in approximately 15 mm loss of aperture, and thus the magnet aperture dimensions must be increased to accommodate it, therefore reducing the magnetic field strength for a given current (see section 4). Carefully radiused conductors are inserted into the slots: the alumina tube acts as a support for these conductors and in addition provides high-voltage insulation. At one end of the alumina tube there is capacitive coupling between the beam screen conductors and an outside metallization, which is connected to a metallic cylinder that is at ground potential (Fig. 14). The capacitive coupling provides a continuous path for the beam image current while preventing eddy-current loops: eddy-current loops can significantly increase field rise time. Three-dimensional electromagnetic simulations have been carried out to optimize the geometry of the beam screen. Nevertheless the design of the upstream end of the beam screen (Fig. 17), results in an open-ended half-wavelength resonator; this is due to the region where the screen conductors overlap with the outer metallization [52].

Each MKI kicker magnet has toroidal ferrite rings mounted around each end of the alumina tube, outside of the aperture of the kicker magnet (Fig. 16). The original purpose of the rings mounted on the end where the screen conductors are connected directly to the beam pipe was to damp low-frequency resonances [53].

During long shutdown 1 (LS1) of the LHC, the beam screen of the MKI kicker magnets was upgraded to have 24, rather than 15, screen conductors [53]. *CST* simulations also show that the longitudinal distribution of volume losses of the post-LS1 MKI kicker magnets is non-uniform: the power deposition in the yoke is predominantly at the capacitively coupled end of the magnet, with losses being relatively low in the down-stream half of the yoke [52]. The design of the upstream end of the beam screen and ferrite rings can be optimized to reduce the beam-induced power deposition in the ferrite yoke, at the expense of increased power deposition in the upstream ferrite rings: nevertheless, redistributing power deposition in this way can be advantageous (see section 5.6).
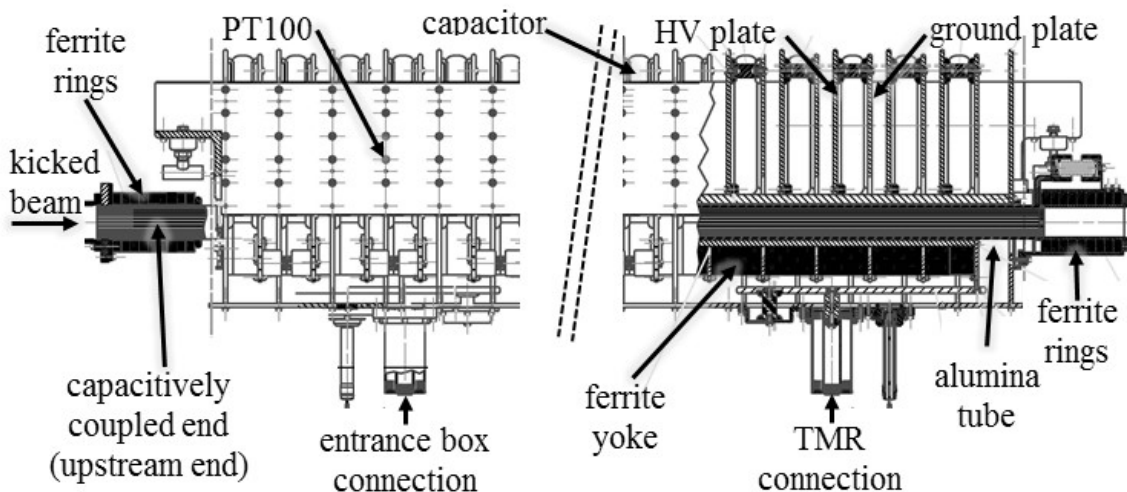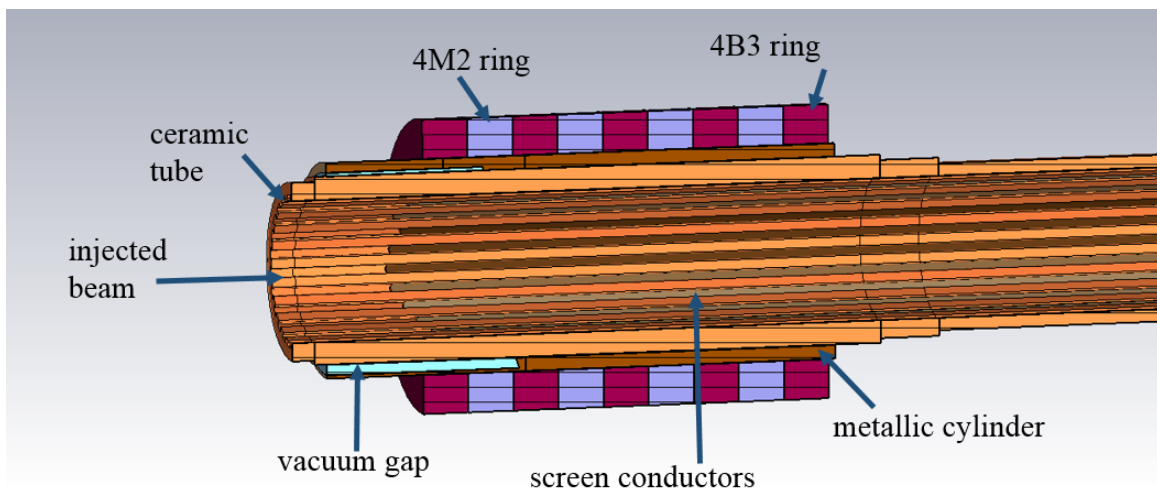

Fig. 16: MKI kicker magnet

Since the MKE and MKI beam screens (serigraphy for the MKE kicker magnets and conductors for the MKI kicker magnets) are in the beam aperture, a fast changing magnetic field (during field rise and fall) induces a high voltage on the beam screen. The magnitude of voltage induced is dependent

upon the position of the conductor in the aperture of the kicker magnet. For the MKI kicker magnets, extensive 3D electromagnetic simulations have been carried out, using the code TOSCA [16], to study electric fields on the surface of the alumina tube. The predictions, in conjunction with operational experience, are used to determine a safe upper operating limit for the electric field [54, 55]. Based on the results of these simulations, the electric field gradient associated with the conductors at highest voltage is reduced by optimizing the length of the screen conductors, such that those at lower voltage 'shade' those at higher voltage [40]: hence, as shown in Fig. 17, the screen conductors towards the HV busbar (bottom) of the alumina tube have the shortest length. In addition, a vacuum gap was introduced between the outside of the alumina tube and the metallic cylinder (Fig. 17), to significantly reduce the electric field at this end of the screen conductors [54]. As a result of the high permittivity of the alumina tube, this gap reduces the capacitance of the capacitively coupled end of the beam screen and hence causes the half-wavelength resonances, resulting from the overlap of the screen conductors with the metallic cylinder, to increase in frequency [56].

Fig. 17: Upstream end of beam screen of MKI kicker magnet

In summary, the design of a beam screen must be optimized for achieving the required field rise/fall time, good high-voltage behaviour, and reducing the real part of the longitudinal beam-coupling impedance over a broad frequency range. The real component of longitudinal beam-coupling impedance can be significantly reduced by:

– incorporating a metallized alumina chamber;
– silver serigraphy of ferrites (painted fingers): there is negligible loss of aperture, but a high impedance resonance is introduced by the serigraphy;
– include beam screen conductors within the kicker magnet aperture: however this can result in approximately 15 mm loss of aperture and is thus usually not applicable as a retrofit to an existing kicker magnet;
– using striplines instead of a ferrite loaded magnet: Fig. 15 shows that the DAΦNE striplines had a very low longitudinal impedance [57]. However using striplines is not feasible for obtaining a large deflection angle in a limited length.

Even with a well-designed beam screen, with high bunch intensity and short bunch lengths, integrated over many hours of a good physics fill, the beam-coupling impedance of the kicker magnet yoke can lead to significant beam induced heating of the yoke: thus, enhanced cooling may be necessary.

5.6   Yoke temperature

5.6.1   Cooling

To limit longitudinal beam-coupling impedance, while allowing a fast magnetic field rise time and good high-voltage behaviour, a beam screen can be included in the aperture of the kicker magnet (section 5.5). Nevertheless, the beam screen may not sufficiently limit beam-induced heating of the yoke. If the yoke exceeds its Curie temperature it temporarily loses its magnetic properties, preventing further injection/extraction until the yoke cools down: because of a long thermal time constant this could require several hours [32]. Kicker magnets are frequently installed in vacuum: convection is negligible and, depending upon the emissivity of the inside of the vacuum tank, thermal radiation is limited [58, 59].

To limit the temperature rise of the SPS extraction kicker magnets, due to beam-induced power deposition, the ferrite yoke is indirectly cooled using water [29, 60]. The cooling is implemented using water-cooled aluminium nitride plates, which are in thermal contact with the ferrites: aluminium nitride is a good thermal conductor but is also electrically insulating, which is necessary as the ferrite is at pulsed high voltage. The cooling allows the beam-induced power deposition to be doubled, with respect to a non-cooled system, before the Curie temperature of the ferrite yoke is reached [29].

For the MKIs, as a result of the low thermal emissivity of the internal surface of the vacuum tanks [58], cooling of the ferrite yoke by thermal radiation is limited. Hence, High Luminosity LHC (HL-LHC) type beam would result in temperatures of the upstream ferrite yokes and upstream ferrite rings well above their Curie temperatures [61], despite the presence of an effective beam screen. Thus extensive research has been carried out to find a high emissivity coating, for the internal surface of the vacuum tank, which is compatible with ultra-high vacuum, thermal bake outs, and high voltage, and does not peel or flake. Several surface finishes have been considered: laser treatment, carbon coating, multilayer optical coatings deposited by magnetron sputtering, and coatings deposited by thermal spray (e.g., plasma spray and flame spray). However, although increasing the emissivity reduces both the maximum temperature and the thermal time constant, so that the yokes cool down more rapidly, the temperatures are not reduced sufficiently for HL-LHC type beam [61]. Hence, other cooling schemes have been studied.

Aluminium nitride plates in good thermal contact with the ferrite yoke have also been studied: predictions show that the yoke would be below its Curie temperature. However, *CST* simulations show that the ferrite rings, at the upstream end of the kicker magnet, experience a significant proportion of the total beam-induced power deposition, for a structure that has relatively little volume. Hence additional cooling is required for the upstream ferrite rings as their temperatures are otherwise predicted to exceed their Curie point: these rings already have a relatively high Curie temperature of 200°C and 250°C for 4M2 and 4B3 ferrite, respectively [61].

Recent beam-coupling impedance studies show that a change in the design of the upstream end of the magnet can reduce significantly the beam-induced power deposition in the ferrite yokes by moving it into the upstream ferrite rings (see section 5.5). Detailed *ANSYS* simulations show that, with this new proposed design, for HL-LHC type beam, the high temperature of the upstream yokes is caused mainly by the heat conducted and radiated from the ferrite rings. Thus, effective cooling of the ferrite rings significantly reduces the temperature of the upstream ferrite yokes too [61]: direct cooling of the ferrite rings is possible as they are not at pulsed high voltage. Nevertheless, the cooling system will be in a pulsed high voltage and ultra-high vacuum ($<10^{-9}$ mbar) environment: hence, one must ensure that the risk of liquid leakage into machine vacuum is negligible.

5.6.2   Measurement of yoke temperature

PT100 temperature sensors are used in several of the kicker magnets installed in the CERN accelerator rings: these are generally shielded to avoid beam induced electromagnetic interference. The

PT100 sensors cannot be in direct contact with the magnet yoke, as the yoke is at pulsed high voltage [32, 60]: hence, during operation, the temperature indicated by a PT100 may be significantly less than the actual yoke temperature. In addition, for the MKIs, the temperature distribution throughout the yoke is highly non-linear [52, 61]. Thermal studies have been carried out to correlate temperatures measured by the PT100s with the yoke temperatures. However, there is always an uncertainty because this correlation is also dependant on the heating and cooling rates, which varies during LHC operation.

Either 8C11 or CMD5005 ferrite is presently used for the MKI yoke: the permeability rapidly reduces for temperatures above the Curie temperature (~125°C). In addition to reducing the strength of the magnetic field, a decrease in the inductance of an MKI results in a decrease in the propagation delay of the kicker magnet and the rise time of the current in the TMR. By pulsing the MKI magnets without beam in the accelerator, the propagation delay of a magnet and the rise time of the current in the TMR can be measured: this is carried out immediately after beam in the LHC is dumped—when, after a long duration physics run with high intensity beam, the yoke of the MKIs is still relatively warm. *PSpice* simulations, where the inductance or capacitance of every cell is modelled as reduced by a given percentage, show that the percentage reduction of magnet delay is almost five times greater than the percentage decrease in TMR current rise time: hence, the magnet delay is the preferred of the two diagnostics. In general, a plot of magnet propagation delay versus measured temperature, or TMR current rise time versus measured temperature, is relatively linear: however once the ferrite starts to lose its permeability, there is a relatively rapid increase in the slope of the curves. Hence, these electrical measurements allow one to deduce whether or not the ferrite yoke is approaching/above the Curie temperature [62].

5.7 Electron cloud

Significant pressure rise, due to electron cloud, occurs in and nearby the MKIs (Fig. 18): the predominant gas desorbed from surfaces is H_2. Conditioning of surfaces reduces electron cloud, and thus dynamic pressure rise, but further conditioning is often required when beam parameters (e.g., bunch spacing, length, and intensity) are pushed.

Voltage is induced on the MKI screen conductors during field rise (to 30 kV) and fall (to −17 kV) [54]. High pressure, at the upstream (capacitively coupled) end, can result in breakdown/flashover. Hence, it is desirable to minimize dynamic pressure in and around the MKIs. The alumina tube of each MKI has a secondary electron yield (SEY) of ~10 when first installed and, together with metallic surfaces facing the beam, requires conditioning with beam [63].
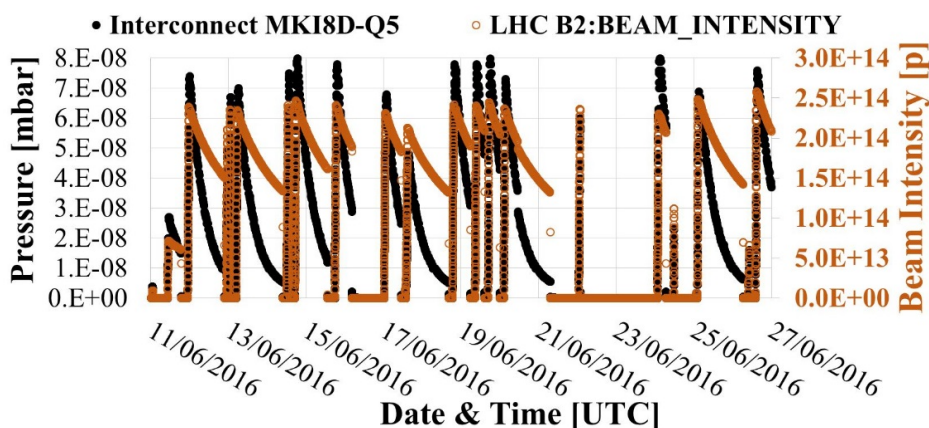
Fig. 18: Example of dynamic pressure in an MKI8D interconnect and beam intensity during June 2016

In order to mitigate electron multipacting, a coating of Cr_2O_3 is applied, by Polyteknik (Denmark), to the inside of the alumina tube by magnetron sputtering. Measurements show that naked, high-purity, alumina has a maximum SEY (δ_{max}) of ~9. A Cr_2O_3 coating, applied by magnetron sputtering, reduces

δ_{max} to approximately 2.3: bombarding the surface with electrons further reduces δ_{max} to less than 1.4 (Fig. 19) [63]. In addition, a set of samples sputtered with 50 nm of Cr_2O_3 was installed in a setup in the CERN SPS, during the winter stop of 2016−2017, for tests with beam. These tests confirmed that relatively rapid conditioning of the Cr_2O_3 occurred in the presence of beam.
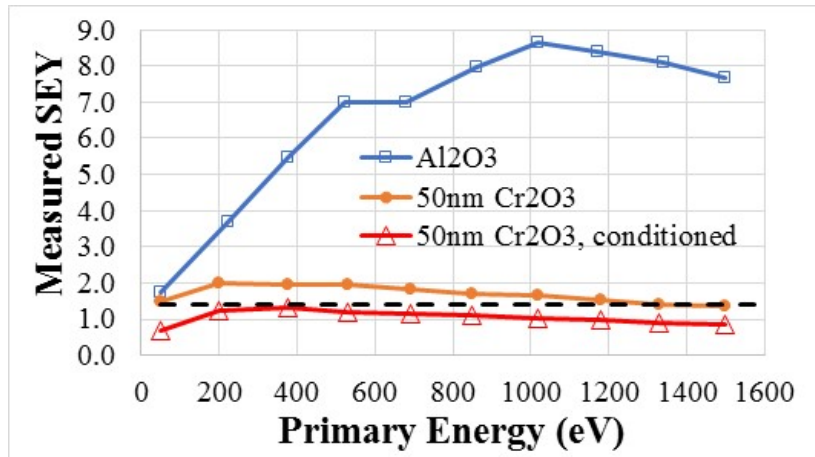
Fig. 19: Measured SEY of high purity alumina and alumina with a 50 nm Cr_2O_3 coating: bombarding Cr_2O_3 with electrons reduces δ_{max} to below 1.4.

Cr_2O_3 was originally studied, for coating of the inside of an MKI alumina tube, based on papers published by Sudarshan and Cross [64] and by Shioiri [65], which reported a ~30% increase in voltage of surface flashover in vacuum, in comparison with uncoated alumina. Reference [65] concludes that the effectiveness of Cr_2O_3, at increasing surface flashover in vacuum, is due to:

- a reduction in secondary electron avalanche;
- a reduction of surface charging due to decreased surface resistance (10^{10}–10^{11} Ω·cm).

5.8 Pulse-forming line/network

The simplest configuration for a pulse-forming circuit is a PFL (transmission line/coaxial cable). The PFL gives fast and ripple-free pulses, but low attenuation is essential, especially with longer pulses, to keep droop and 'cable tail' within specification [3]. Attenuation is adversely affected by the use of semiconductor layers to improve voltage rating [3]. Hence, for PFL voltages above 50 kV, SF6 pressurized polyethylene (PE) tape cables have been historically used: however the availability of SF6 gas filled coaxial PFL cables is a concern for both existing and future kicker systems. PFL becomes costly, bulky, and the droop becomes significant ($\geq$ 1%) for pulses exceeding approximately 3 µs duration.

Where low droop and long pulses are required, a PFN is used: a PFN is an artificial coaxial cable made of lumped elements. The SPS extraction PFNs at CERN [66], which are approximately 40 years old, have approximately 20 cells, connected in series in a single line (Fig. 20, RHS), which are individually 'adjustable': these PFNs have 'corners' (Fig. 20, LHS), therefore mutual inductance between cell inductances is not well defined and can result in ripple on the pulse. Adjusting the pulse flat-top is difficult and time consuming.
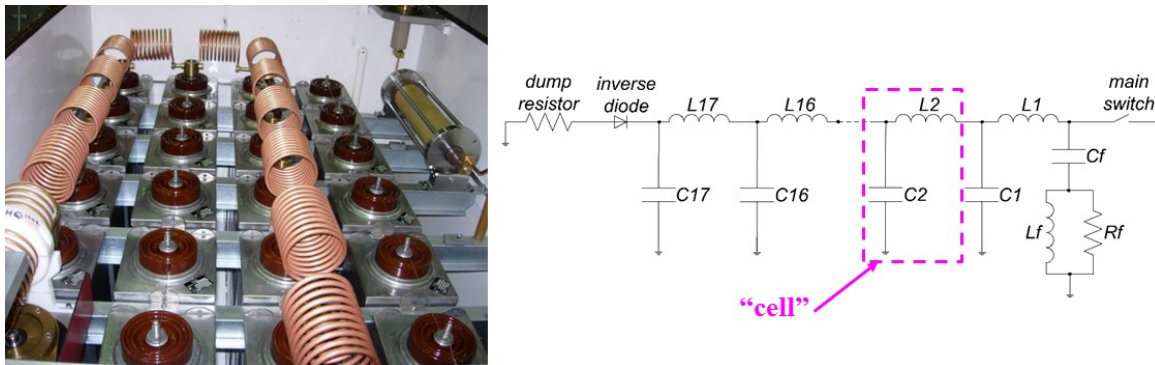
Fig. 20: The SPS extraction PFNs at CERN have approximately 20 cells, which are individually 'adjustable'

The preservation of the transverse emittance of the proton beam at injection into the LHC is crucial for luminosity performance. The transfer and injection process is important in this respect, and injection offsets are a well-known source of error [67]. To limit the beam emittance blow up due to injection oscillations, the reflections and the flat-top ripple of the field pulse must be lower than ±0.5%, a very demanding requirement [9].

Each of the two LHC injection kicker systems has four 5 Ω PFNs [68]. Each PFN consists of two lumped element delay lines, each of 10 Ω, connected in parallel [68]. Each 10 Ω line consists of 26 central cells plus two end cells. A cell consists of a series inductor, a damping resistor connected in parallel, and a capacitor connected to ground (Fig. 21, LHS). The inductors are part of a single continuous coil, 4.356 m long, with 198 turns and a pitch of 22 mm [68]. The central cell inductors are made of seven turns each. The nominal MS and DS end-cell inductors have nine turns and five turns respectively, but are built with one extra turn to allow some adjustment to compensate for end effects. The 26 central cells of the coils are not adjustable and therefore are defined with high precision: the coil conductor is a copper tube wound on a rigid fibreglass coil former. Both delay lines are mounted in a rectangular tank (Fig. 21, RHS), with mild steel walls, that is filled with insulating silicone fluid. Each line is surrounded by a 3 mm thick, Ω-shaped, aluminium shield, which has an inner radius of 140 mm. Two thyratron switches, a MS and a DS, are connected to the PFN (see also Fig. 4).
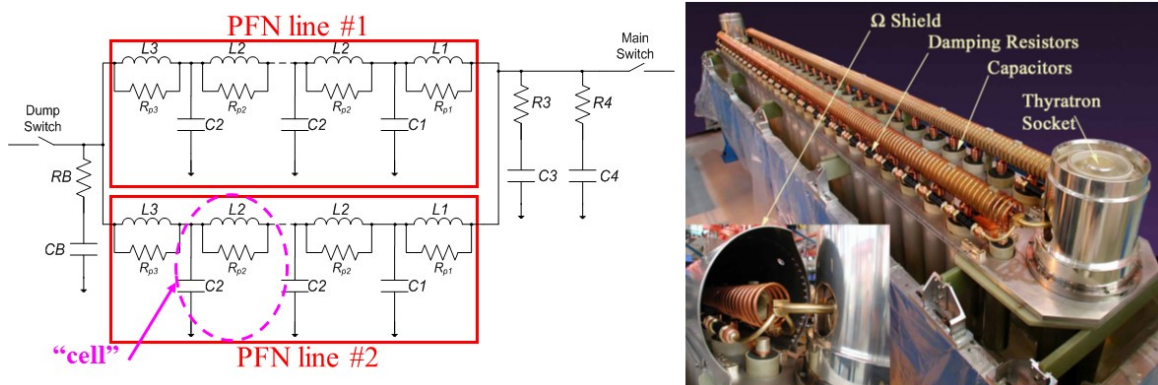

Fig. 21: Each LHC injection PFN consists of two parallel 10 Ω lines with precision wound coils
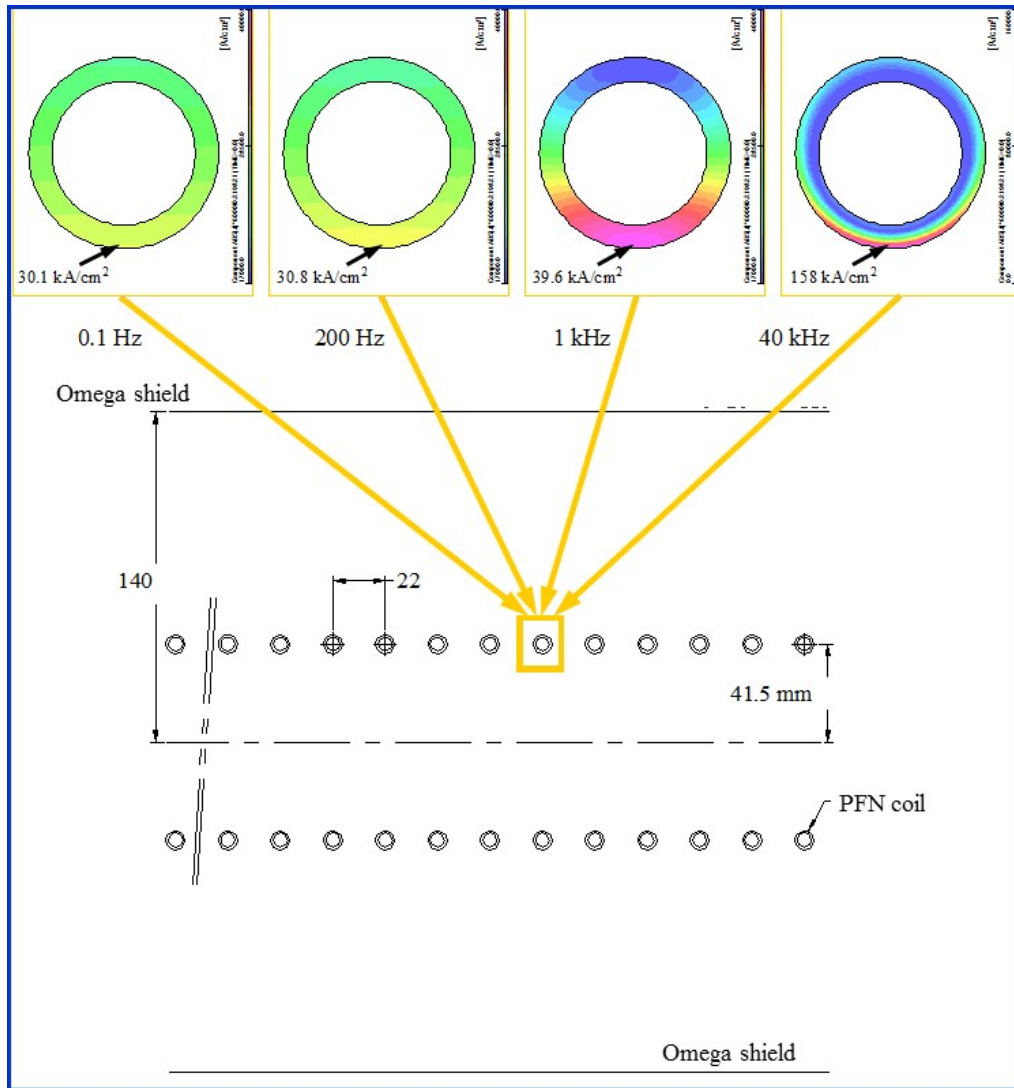
Fig. 22: *Opera2D* prediction for current distribution in LHC injection PFN for a current of 6 kA

Opera2D simulations have been carried out to assess the frequency dependence of inductance and resistance of the coil of the LHC injection PFN [19]. Figure 22 shows the predicted current distribution in the PFN coil at frequencies of 0.1 Hz, 200 Hz, 1 kHz, and 40 kHz: the nominal DC current density is 27.3 kA/cm^2, for a total current of 6 kA.

Figure 23 shows the predicted inductance of a 7-turn cell versus frequency for a mean radius of the coil of 41.5 mm. The 'Grover limits' refer to values calculated from equations [19]. The reduction in inductance as frequency is increased from DC to a few hundred Hertz is mainly due to shielding attributable to the Ω-shield. The reaction field from the eddy currents induced in the Ω-shield reduces the flux density along the axis of the coil from 0.343 T near DC to 0.315 T at a few hundred Hertz, for a current of 6 kA. As the frequency is increased beyond a few hundred Hertz the inductance decreases, mainly due to skin effect and proximity effect within the coil. Conduction losses along the PFN coils result in a droop of the pulse of approximately 0.5% in the kicker magnet. *PSpice* simulations, subsequently confirmed by measurements, show that conduction losses in the PFN coil can be compensated for by increasing the PFN capacitor values linearly from the MS end to the DS end [68].
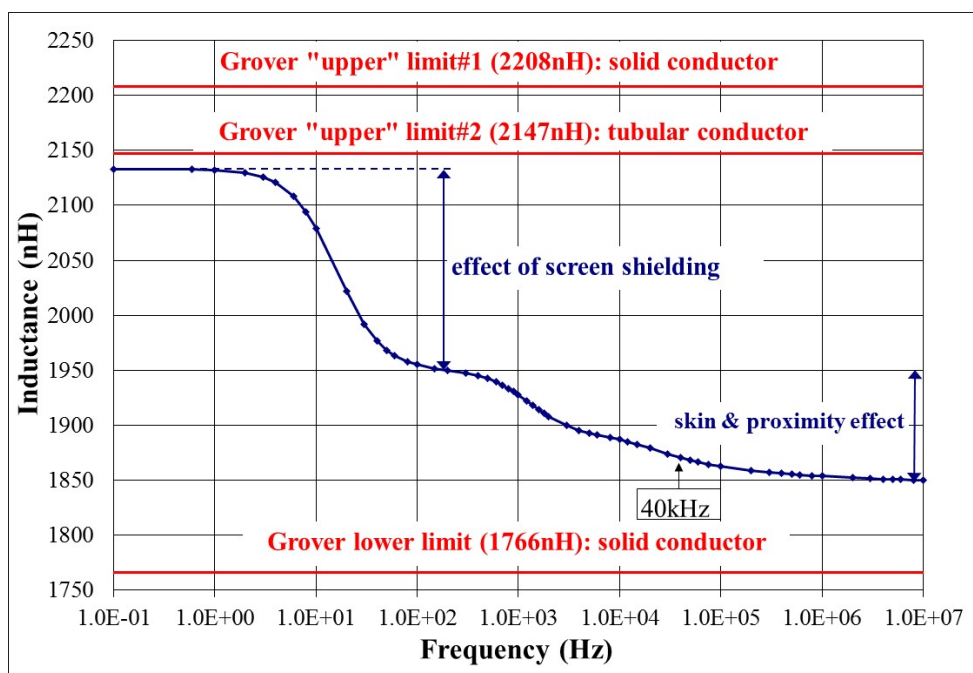
Fig. 23: *Opera2D* prediction for inductance of a 7-turn PFN cell, versus frequency, for a mean radius of the coil of 41.5 mm.

5.9   Power switches

5.9.1   *Thyratrons*

Despite the advances in high-power solid-state switches, deuterium thyratrons are still widely used as the power switch in kicker systems. The deuterium thyratron is a high peak power device, which uses deuterium gas as the switching medium. The switching action is achieved by a transfer from the insulating properties of neutral gas to the conducting properties of ionized gas [69]. Voltage breakdown in the deuterium-filled gap is initiated by free charges (electrons and ions) crossing the gap under the influence of an electric field. If sufficient energy is available, gas molecules are ionized producing more free charges. The positive ions are accelerated towards the lower potential electrode and cause the release of secondary electrons. Under the right circumstances, the processes become self-sustaining and voltage breakdown occurs [69].

Thyratron commutation is achieved by introducing plasma into the grid/anode region via slots in the grid structure. The plasma is created in the cathode/grid region by a fast-rising trigger pulse applied to the grid(s), which then diffuses to the grid slots where it comes under the influence of the anode field [69].

Three-gap thyratrons can hold off 80 kV and switch 6 kA of current with a 30 ns rise time (10% to 90%) [~150k A/μs]. The individual gaps in a three-gap thyratron break down in sequence [70, 71]. Initially the gap closest to the cathode conducts and the full PFN voltage is shared between the centre and anode gaps. Approximately 50 ns later the centre gap starts to conduct and the full PFN voltage builds up across the anode gap [70]. The voltage redistribution between the parasitic capacitance of each of the gaps is associated with a flow of displacement current [71]. The displacement current also flows in the external circuit, and hence through the kicker magnet, and can increase the effective rise time of the kick [72]. Appropriately placed saturating inductors can be used to reduce both the effect of the displacement current and the rise time of the main current pulse [71, 73].

Special care must be taken with the high-power thyratron:

- coaxial housings are used to achieve low inductance but there must be adequate insulation to the housing;

- current flow in the connections around the thyratron should be symmetrical. An asymmetrical magnetic field can impose forces on the internal plasma preventing uniform current density which may affect performance and lifetime [69];

- the appropriate thyratron must be selected (e.g., suitable rating for peak current and average current) and properly applied for the anticipated short circuit and fault conditions;

- the thyratron must be adequately cooled to ensure that the maximum specified envelope temperature is not be exceeded;

- erratic turn on (turn on without a trigger being applied) can result in operational problems: erratic turn on is reduced significantly by 'fast' (~ms) charging of the PFN/PFL immediately before the kicker magnet is required to be pulsed (see below);

- the reservoir voltage of the thyratron should be optimized. The gas density in the grid/anode gap must be maximized, to minimize current rise time and switching losses and maximize thyratron lifetime, consistent with achieving a low rate of erratic turn on.

In order to reduce as much as possible the number of erratic turn ons, RCPSs are used to charge PFNs for kicker magnets [3, 74]. The number of erratic turns on of a thyratron switch is dependent upon several variables, which include the duration for which there is a high voltage across the thyratron; thus, in order to minimize the number of erratics, it is advantageous to minimize this time period. In general, an RCPS can also allow the reservoir voltage to be increased, if the rate of erratic turn on is still acceptable, and therefore help to extend thyratron lifetime.

The fast RCPS developed for the LHC injection kicker systems charges two PFNs to 54 kV in approximately 800 μs: approximately 600 μs later the PFNs can be discharged into the kicker magnets [75]. However, in reality, the LHC injection PFN are fully charged for between 2 ms and 3 ms before the MSs are triggered. During 2015 and 2016, for the eight LHC injection kicker magnets, there was a total of approximately 250,000 MS thyratron injection pulses, one of which resulted in a MS thyratron erratic during resonant charging [63].

To achieve significantly improved performance and lifetime a thyratron can be double pulsed to turn it on: the first pulse, applied to grid 1, pre-ionizes the cathode grid space, which prepares the cathode region for conducting the main current pulse. The second pulse, which is applied to grid 2, should be delayed by at least 500 ns with respect to the first pulse, provides a fast rising voltage to ensure precise triggering (1−2 ns) of the thyratron [69].

As mentioned in section 5.2, the length of the pulse in the kicker magnet can be controlled in length, between 0 and $2\tau_p$, by adjusting the timing of the thyratron DS (Fig. 4) relative to the thyratron MS. However, the wavefront generated by the DS turn-on must travel through the PFL/PFN: as a result of attenuation and dispersion in the PFL/PFN, once the wavefront reaches the MS it has a slower falling edge than the corresponding rising edge that was generated by the MS turn on. Hence, the field fall time of the kicker magnet would be longer than the rise time. If a fast field fall time is required a 'clipper switch' thyratron can be used: this thyratron would be connected from the PFN/PFL side of the MS to ground. This clipper switch can also be used to reduce the duration of the field pulse; hence, the DS thyratron would typically be replaced with an inverse diode. An example of a clipper switch, combined with an inverse diode at the remote end of a PFN, is shown in reference [76].

Control of the duration of the field pulse, either by a DS or a clipper switch, can also be an important protective measure during a fault condition. For example, for the LHC injection system, if there is an erratic (untriggered turn on) of an MS thyratron, already circulating beam could be miskicked: hence, in case of an MS erratic in this system, the remaining MS thyratrons and all the DS thyratrons,

of the same system, are triggered: triggering the DS thyratrons reduces the field pulse duration and hence the potential number of bunches which are miskicked.

As mentioned above, a thyratron switch is susceptible to erratic (uncontrolled) turn on, which can result in circulating beam being miskicked and hence may cause considerable damage to accelerator components. Power semiconductor switches potentially have advantages, over thyratrons, of reduced erratic rate, increased lifetime, and reduced maintenance.

5.9.2   *Power semiconductor switches*

Despite progress in the capabilities of fast semiconductors switches, they still have limited voltage and/or current capability in comparison with thyratrons. In addition, semiconductors may be influenced by ionizing radiation and neutron flow. Depending on the type of radiation, the semiconductor component type and its working conditions, the radiation effects can be cumulative with relatively slow deterioration of semiconductor performance and/or sudden malfunction or failure: the latter is called single event effects (SEE) [77, 78]. The cumulative effects, which result from total ionizing dose and displacement damage, are responsible for the modification of component parameters such as leakage current, bipolar transistor gain, opto-coupler efficiency, field-effect transistor (FET) threshold voltage, voltage reference value, etc. On the other hand, a SEE provokes sudden malfunctions, which, in the case of HV power semiconductors, usually leads to component failure: this is known as single event burnout (SEB) [79-81]. For a given radiation dose the SEB rate is strongly dependent on the applied voltage: there is a very steep increase of the failure rate when the applied voltage is higher than a certain percentage of the components' rated voltage. The general recommendation for high voltage components, to maintain a reasonably low SEB rate, is to apply a maximum DC voltage of approximately 50% of the semiconductor rating. For the LHC abort kickers (section 5.9.2.1) the power semiconductors can be affected by radiation and neutron flow from the LHC [77].

Presently a range of power semiconductors are either in use in the pulse power generators of various kicker systems at CERN, or are in prototype generators. A number of examples of applications are described in the following sections.

5.9.2.1   *LHC dump (abort) kicker system*

In some applications thyratron switches cannot be used, e.g., for the dump (abort) kickers in the LHC where no self-firing is allowed [82]. The nominal LHC beam consists of 2808 bunches per beam, with 1.5×10^{11} protons per bunch. Once accelerated to 7 TeV the stored energy per beam is 470 MJ. A beam dump, an 8 m long graphite block, is the only element that can safely absorb this energy. The LHC beam dumping system (LBDS) must protect the LHC from damage by reliably and safely extracting and absorbing the circulating beams when requested. The LBDS consists, per beam, of 15 horizontally deflecting extraction kicker magnets (MKD), 15 vertically deflecting septum magnets and 10 dilution kicker magnets (MKB), followed by several hundred meters of beam transfer line before the extracted beam reaches the dump block [83].

The MKD kicker system is the most safety critical and complex element of the LBDS as a fault in the system can lead to significant damage of LHC equipment. The extraction of the beam from the LHC is at a fixed angle of 0.275 mrad, by the MKD magnets, hence the MKD system needs to track the beam energy (between 450 GeV and 7 TeV). The maximum operating voltage of the MKD system is 30 kV to generate a pulsed current of 19 kA with a flat top of 95 μs. The MKDs should not turn on erratically during LHC operation, and must reliably switch on within a 3 μs particle-free abort gap when required [84]. To minimize spontaneous self-triggering, semiconductors are used for the power switches: fast high current thyristors, from ABB and Dynex, are utilized. The semiconductor switches permit the required wide dynamic range of operation [82].

Each semiconductor switch module for the LHC abort kickers consists of ten series gate turn off (GTO) thyristors (Fig. 24) that have been optimized for turn on. The maximum forward voltage rating of each GTO is 4.5 kV and the switch module is operated over a voltage range from 2.2 kV (450 GeV) to 30 kV (7 TeV) [82]. The current switched is in the range from 1.2 kA to 19 kA: the specified maximum rate of rise of current is 20 kA/μs, which corresponds to ~1/8th of the capability of a thyratron. However, recent tests on similar GTOs, with a high-current gate drive, have demonstrated a capability of more than 32 kA/μs. In order to achieve high reliability each generator has 2 parallel branches, either of which can carry full load current. At least 14 out of the 15 kicker magnets must operate simultaneously on request to safely extract the beam from the LHC. Any spontaneous firing or fault of one of the pulse generators is detected and the other generators are triggered [82].

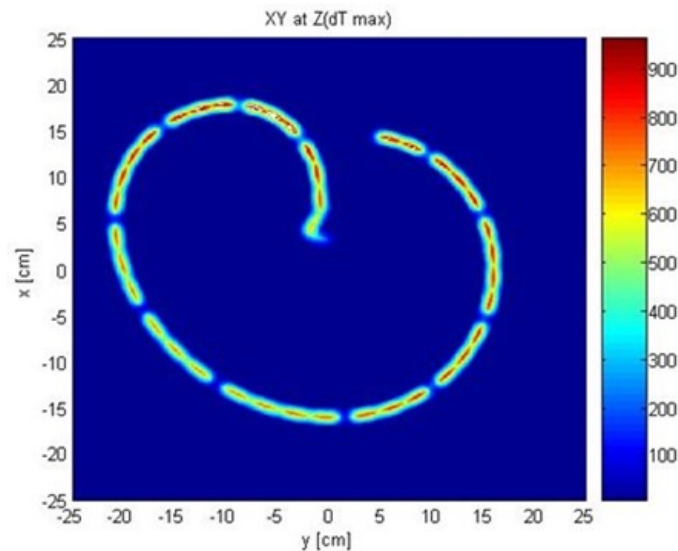**Fig. 24:** Stack of-high power GTOs (LHS) and individual GTOs (RHS)

Fig. 25: Lissajous figure of LHC extracted beam on the dump block – right hand side scale shows temperature (°C).

The function of dilution kickers is to sweep the extracted beam in a Lissajous figure (Fig. 25) on the dump block: the circumference of the Lissajous figure is approximately 1.2 m. Separate horizontal

and vertical MKB systems are used to generate sine and cosine-like current shapes over 90 μs. The peak deflection angle is 0.28 mrad (for 450 GeV to 7 TeV beam). Each MKB generator comprises a capacitor coaxially connected to the magnet inductance. The capacitor is discharged through a solid-state closing switch: the discharge pulse is an attenuated sinusoidal oscillation of 24 kA maximum amplitude (at 7 TeV) with a period of 70 μs.
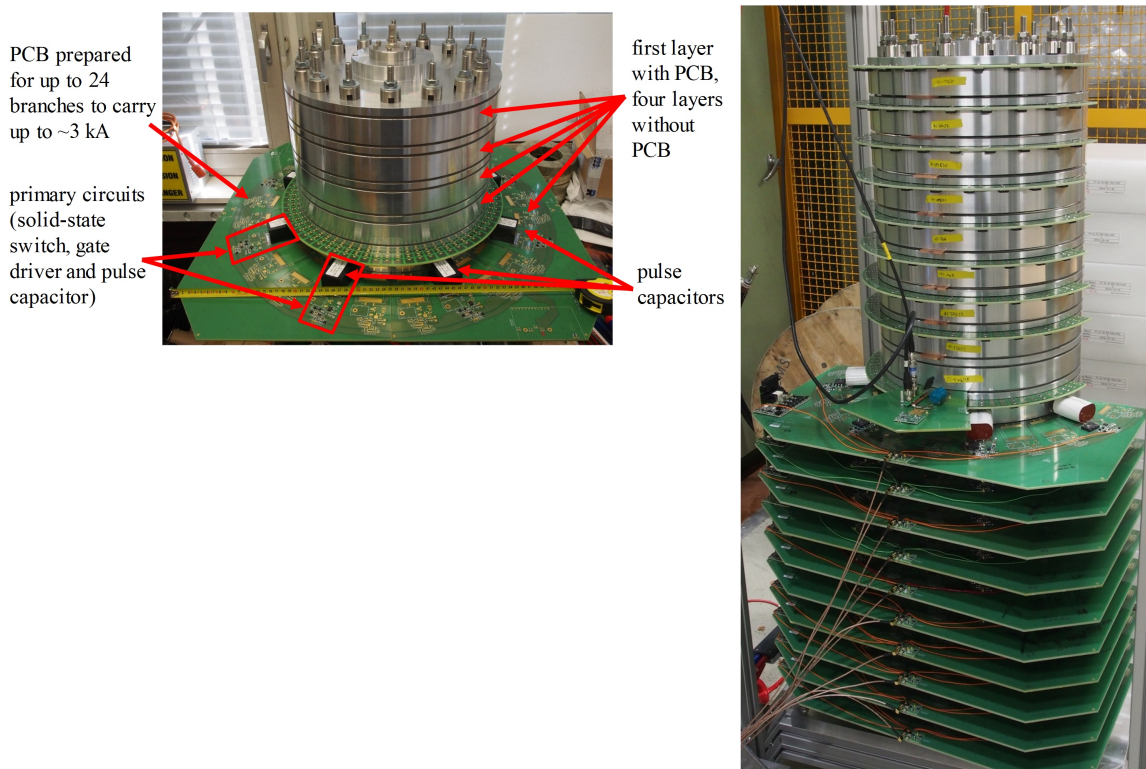
5.9.2.2 Inductive adder

5.9.2.2.1 Compact linear collider damping ring

The compact linear collider (CLIC) would be a high-energy electron−positron collider. It could provide very clean experimental environments and steady production of all particles within the accessible TeV energy range. To achieve high luminosity at the interaction point, it is essential that the beams have very low transverse emittance: the pre-damping ring (PDR) and damping ring (DR) damp the beam emittance to extremely low values in all three planes [85].

Stripline kickers are required to inject beam into and extract beam from the PDRs and DRs [86]. Jitter in the magnitude of the kick waveform causes beam jitter at the interaction point [87]. Hence, in particular, the DR extraction kicker must have a very small magnitude of jitter: the 1 GHz specifications call for a 12.5 kV pulse of 900 ns flat-top duration, with a combined ripple and droop of not more than ±0.02% [85]. An inductive adder (IA) has been selected as a promising means of achieving the specifications for the DR kicker [88, 89]. The IA is a solid-state modulator, which can provide relatively short and precise pulses: it is modular and thus the design can be adapted to other requirements: Fig. 26 shows a simplified electrical schematic of an IA. Photographs of prototype IAs are shown in Fig. 27: the LHS shows a 5-layer IA and the RHS a 20-layer IA.
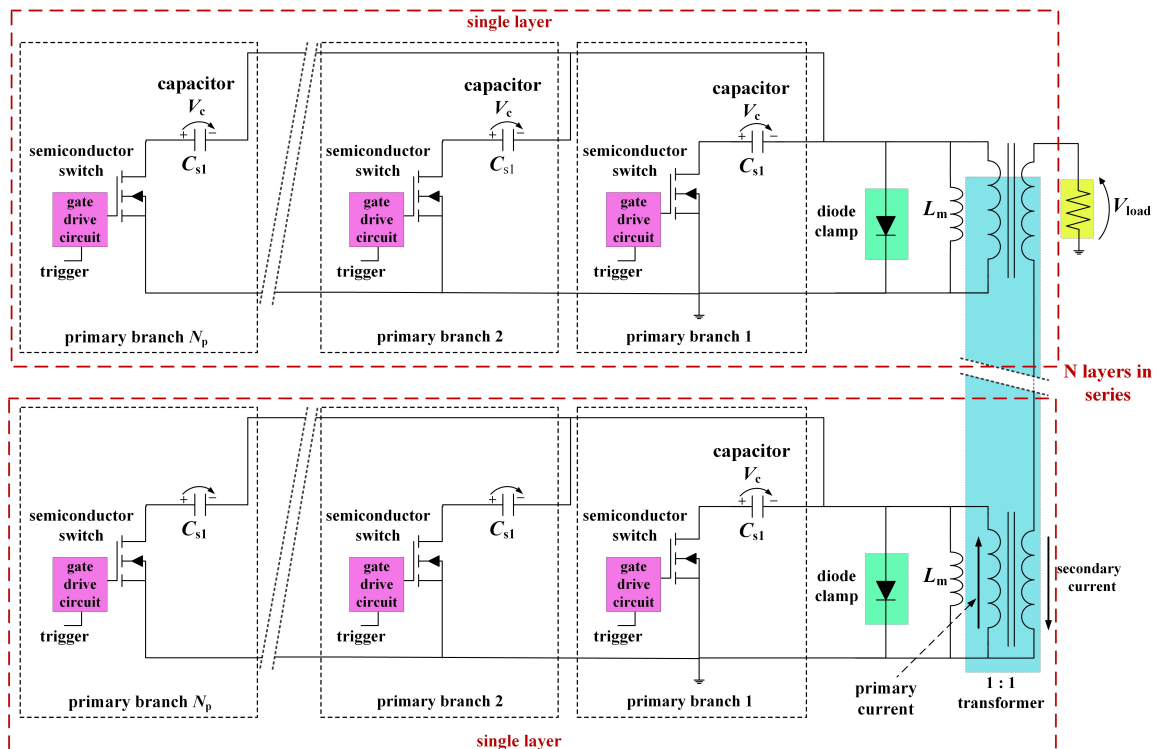
Fig. 26: Simplified schematic of an inductive adder showing N-layers in series on the secondary and Np parallel primary branches per layer.

PCB prepared for up to 24 branches to carry up to ~3 kA

primary circuits (solid-state switch, gate driver and pulse capacitor)

first layer with PCB, four layers without PCB

pulse capacitors

Fig. 27: Prototype inductive adders at CERN: 5-layer IA (LHS) and 20-layer IA (RHS)

An inductive adder (Fig. 26) consists of multiple layers (also known as stages), each of which has a transformer: the transformer usually has a 1:1 turn ratio in order to ensure that it is suitable for fast pulses. The single turn primary totally encloses a magnetic core; hence, the leakage inductance of this geometry is negligible [90]. The secondary winding of each of these transformers is connected in series: hence a step-up voltage ratio of 1:N is achieved by using N-layers, with adequate voltage isolation. The primary circuit typically has many parallel branches: each branch generally contains a single capacitor and a single power semiconductor switch. All the power semiconductor switches and gate drive circuits are referenced to ground and there are no electronics referenced directly to the high-voltage output pulse. In general, the capacitors of all the layers can be charged with a single power supply—this is not, however, necessary and in some applications the capacitors are deliberately charged to different voltages to allow modulation of the output pulse [91].

An IA has good built-in fault tolerance and redundancy, because if one or more solid-state switches of a layer of the inductive adder stack fails to turn on, the magnitude of the output pulse of the IA is reduced by only the voltage of a single layer. However, in order that the failure of one power semiconductor switch does not result in a short circuit on the output of a power supply, and hence failure of the inductive adder to produce adequate output pulses, the capacitors of each layer must be sufficiently decoupled from the power supply using resistors. Similarly a second power supply can be used to provide redundancy in the case of failure of one supply.

Since the IA is of a modular design, extra layers can be added to improve redundancy and/or increase voltage rating. In addition, the modular construction allows for a good scalability, adaption of individual components to the particular application, and a path for future upgrades. A drawback of the IA is that, as a result of it using magnetic cores for the transformer, it has limitations concerning the available pulse duration: however many kicker magnet applications at CERN require pulse durations of only up to 2.6 µs, which is achievable with an inductive adder.

As a result of the low source impedance, the source voltage does not need to be doubled, unlike a matched impedance PFL or PFN. The solid-state switches typically used in the IA are either metal-oxide-semiconductor field effect transistors (MOSFETs) or insulated-gate bipolar transistors (IGBTs). These solid-state switches can be opened when conducting full load current, hence only a portion of the stored energy is delivered to the load during the pulse (therefore a PFL or PFN is not required). In addition, opening of the solid-state switches potentially limits the duration of fault current in the event of a magnet (load) electrical breakdown.

Considerable research and development has been carried out on the IA for the CLIC DR [89]. A significant advantage of the IA over some alternative technologies is the ability to modulate the output [89]. Recent measurements on a prototype IA, equipped with 18-layers including a special analogue modulation layer, are shown in Fig. 28 [92].

Fig. 28 shows the best measured flat-top waveform for two different measurements of an 18-layer IA: the orange curve (top) is an average of 1000 measured pulses and the blue curve (bottom) is an average of 100 measured pulses. The offset difference of the measurements was most probably caused by thermal drift in components or in the high-voltage power supply, which charges the pulse capacitors [92]. For the blue curve, the measured flat-top stability is ±0.03% (±1.80 V) over the full 900 ns flat-top duration, at 6.3 kV. However, the flat-top stability is ±0.02% (±1.35 V) over the first 160 ns and the last 160 ns of the flat-top duration, as labelled in Fig. 28 [92]. This fulfils the CLIC DR requirements for the flat-top stability of the pulse modulator, for both 1 GHz and 2 GHz specifications of the damping rings [85], at approximately a half of the nominal required voltage.
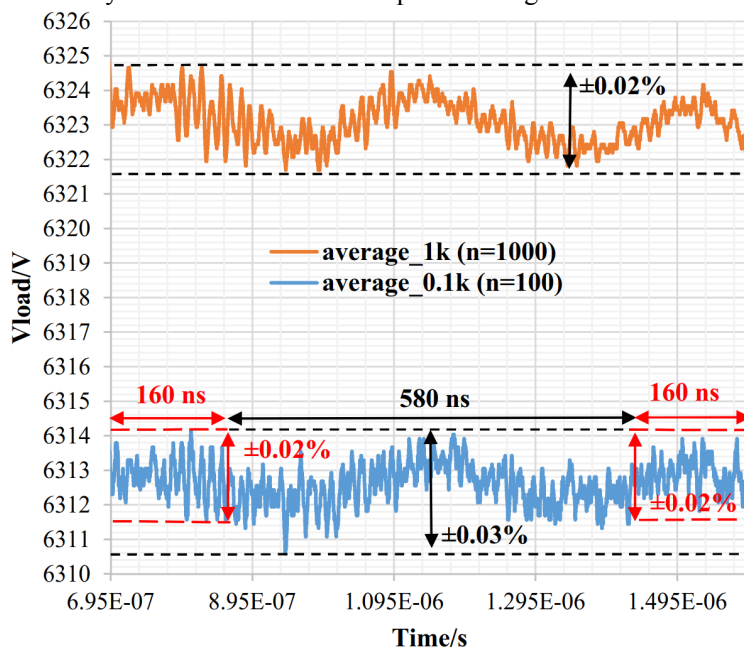

Fig. 28: Measured load voltage with active analogue modulation. The orange curve (top) and blue curves (bottom) are an average of 1000 pulses and 100 pulses, respectively [92].

It should be noted that theoretically a double kicker system can be used to reduce the influence of flat-top ripple upon the beam deflection (see section 5.11).

5.9.2.2.2   CLIC Combiner Ring

The specifications for the CLIC Combiner Ring (CR) extraction kickers call for a burst rate of up to 688 kHz for 140 μs, every 20 ms [85]. The required pulse voltage, of 10 kV into 50 Ω, corresponds to

200 A. The rise and fall time should be no more than 150 ns and the flat-top pulse duration will be between 245 ns and 450 ns, with 96 pulses per burst. Hence, the average repetition rate is 4.8 kHz [93].
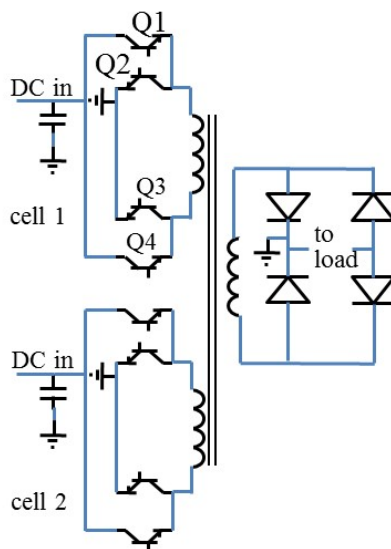
Fig. 29: Novel variant of the typical IA, employing a full-bridge inverter [93]

The energy transferred during a pulse is approximately 1 J, depending upon the flat-top duration, which corresponds to 96 J per burst. The maximum allowable droop during the burst is ~0.25%, corresponding to 25 V. If this energy were stored in a single capacitor, the 10 kV capacitor would need to store at least 19 kJ, which requires a large capacitance value (384 μF). An alternative approach is to use an inductive adder with appropriate droop correction. Assuming that the magnetic core used for the IA must support the voltage × time integral of a burst, this corresponds to a total of ~0.6 V·s. Assuming a 0.5 T saturation flux density for the magnet material, this gives a total cross-sectional area of the core of ~1.2 m^2 [93], which is very large. To reset the cores during the burst, between pulses, requires a reset current of ~100 A, which is similar to the magnitude of the pulse current.

Collaborators at Stanford Linear Accelerator (SLAC) developed a novel variant of the IA topology, employing a full-bridge inverter: Fig. 29 shows a two-cell example. The two cells produce alternating positive and negative polarity pulses, but the load output is single polarity. The flux alternates in direction in the magnetic core: hence, the required cross-sectional area of core material can be reduced by almost two orders of magnitude. Tests and measurements on an initial low-voltage prototype show that long pulse trains can be achieved [93].

5.9.2.2.3   FCC Injection

An IA is also being studied for the injection system of a 100 TeV centre-of-mass future circular collider (FCC) study. This IA design is based on silicon carbide (SiC) MOSFET switches [94]. The FCC injection kicker system would need to deflect 3.3 TeV beam, and the required field rise and fall times are 430 ns: to allow a reasonable magnet fill time, the rise and fall times of the current pulse from the generator need to be <75 ns. A potential drawback of the IA is the output transformer and therefore the risk of saturation of the magnetic core. However, with a maximum flat-top pulse duration of 2 μs, for machine protection reasons, the FCC injection kicker can use an IA for the pulse generator.

Although the available length for the kicker magnets is 150 m, for beam impedance and stability reasons it is desirable to use a significantly shorter length, but this increases the current required from the IA. As a compromise, a current of 2.5 kA and a magnetic length of ~30 m have initially been chosen: the corresponding magnet deflection angle is 0.18 mrad [95]. A system impedance of 6.25 Ω has been selected: this results in an output voltage of 15.7 kV for the inductive adder [94].

5.9.2.2.4 CERN PS KFA45

Semiconductor switch technology is being considered for the CERN PS KFA45 kicker system: it is a 45-year old PFL based system and it is becoming very challenging to find a commercial replacement for the 80 kV SF6 gas filled coaxial PFL cables. Initial specifications for a replacement pulse generator for the PS KFA45 system included a current of 1.52 kA with 2.6 μs flat-top duration and a kicker magnet impedance of 26.3 Ω, terminated in its characteristic impedance: during the flat top the allowable droop and ripple is ±2%. The current and impedance correspond to an output voltage of 40 kV for an IA. The nominal single-way delay of the kicker magnet is 35 ns. The required rise and fall times, defined between 1% and 99% of the field pulse, are 46 ns and 96 ns, respectively [96]. Hence, it is presently assumed that fast switching MOSFETs would be required for the power semiconductor switches. However commercially available MOSFETs presently have a maximum voltage rating of 1.2 kV to 1.7 kV: hence in the region of 50 layers would be required for the IA.

Studies have commenced for an IA system to replace the PFL and thyratron switches of the CERN KFA45 system. These simulations show that minimizing the delay of the IA stack is of paramount performance to achieving fast rise time: thus the height of each layer must be optimized, as must the primary inductance and coupling capacitance between primary and secondary. This will require careful consideration and characterization of the magnetic material to be used and the choice and layout of primary components, especially the pulse capacitors and power semiconductor switches [97].

Recent specifications for the CERN PS KFA45 kicker system require that the kicker magnet is terminated in a short circuit: this will double the required current to more than 3 kA. Modifications of the IA are under consideration so that it can operate with a kicker magnet terminated in a short circuit.

5.9.2.3 Marx generator

In a Marx generator n capacitors are charged in parallel from a relatively low-voltage DC power supply, Udc, and discharged in series into the load, producing an output voltage pulse (V_o) with an amplitude approximately equal to the number of stages (n) times the input voltage (Udc), $V_o=n \cdot Udc$, an idea originally developed by Erwin Marx in the 1920s. In the original Marx generator, spark gaps were used to connect the cell capacitors in series, and resistor and inductors between stages were used to limit charging current, and self-discharge paths [98]. With the improvement in solid-state switch characteristics, major progress has been made on the development of Marx generator type topologies based on semiconductors [99−104].
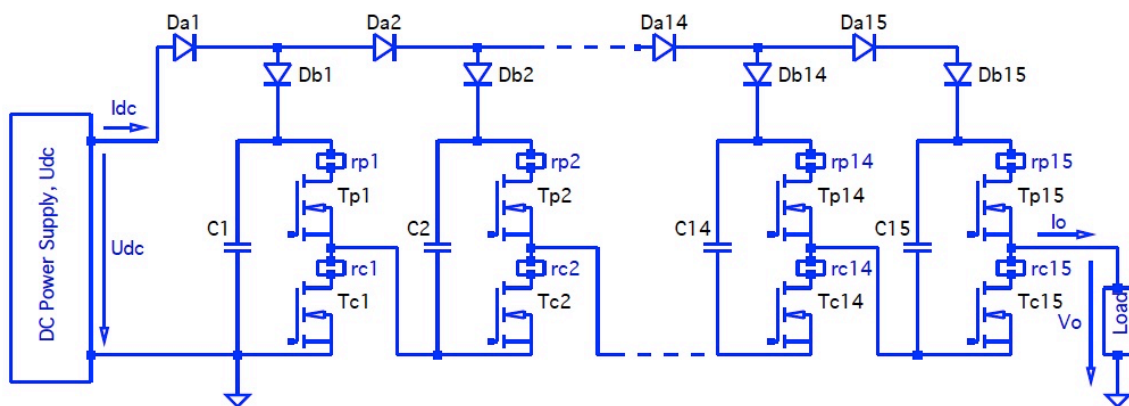

Fig. 30: Simplified schematic of a solid-state Marx generator [105]

The simplest pulse characteristic that a Marx generator can produce is an RC-decay: in this case the capacitance of the erected Marx discharges into a resistive load. The advantage of using the Marx topology, rather than a single capacitor at high voltage, is that the maximum voltage across components

in a Marx cell is the input power supply voltage, *Udc*. Therefore, relatively low-voltage components can be used: since each cell comprises low-voltage components, it is relatively easy to minimize parasitic inductance through the use of closely coupled image planes [99]. In addition, high voltage only exists in the Marx generator when the Marx is erected to produce an output pulse. Also, the energy inside the Marx is stored in several capacitors, instead of one, which has advantages in terms of cost and safety.

Fig. 30 shows a simplified circuit of a solid-state Marx generator [105]. The Marx comprises an energy storing capacitor *Ci*, two set of diodes *Dai* and *Dbi*, and a half-bridge with two MOSFET switches. MOSFETs labelled *Tpi*, where "*i*" is an integer, in the top of the half bridge, apply pulses to the load. The MOSFETs in the bottom of the half-bridge, labelled *Tci*, are for charging capacitors *Ci* between pulses and for defining the falling edge of the output pulse.

One advantage of the Marx generator over the inductive adder is that the Marx does not require magnetic cores to directly generate the output pulse: hence, there is the possibility to generate longer pulses, if the energy stored in the capacitors of the Marx is sufficiently large: this is also dependent upon the permissible droop of the output pulse.

Capacitors *Ci* are charged in parallel from power supply *Udc* through diodes *Dai*, *Dbi*, and MOSFETs *Tci*: during the charging period the load is pulled down to 0 V by turning on MOSFETs *Tci*. The pulse is applied to the load by first turning off MOSFETs *Tci* and then by turning on MOSFETs *Tpi*, to connect capacitors *Ci* in series. The diodes *Dbi* are included for safety reasons, as they limit the discharge of each *Ci* capacitor into the *Ci+1* onwards capacitors, reducing the damage if a *Ci+1* capacitor fails [106].

5.9.2.3.1 CLIC RF breakdown studies

CERN collaborated with *Instituto Superior de Engenharia de Lisboa* (ISEL) and *Energy Pulse Systems* (EPS), Portugal, to develop a high repetition-rate, semiconductor-based, Marx generator. The Marx has been designed to power a spark-gap system: this system allows the study of breakdown rate phenomena for different materials and surface finishes, for RF structures for the proposed CLIC. This Marx circuit is based on SiC MOSFETs, with 15 compact stages, capable of running with capacitive type loads during normal operation, and also in short-circuit mode at reduced repetition rate. The Marx generates pulses of up to 10 kV with widths from 200 ns to 100 μs, at frequencies up to 1 kHz and pulse voltage rise time of less than 100 ns (Fig. 31) with a load capacitance of 150 pF [106].
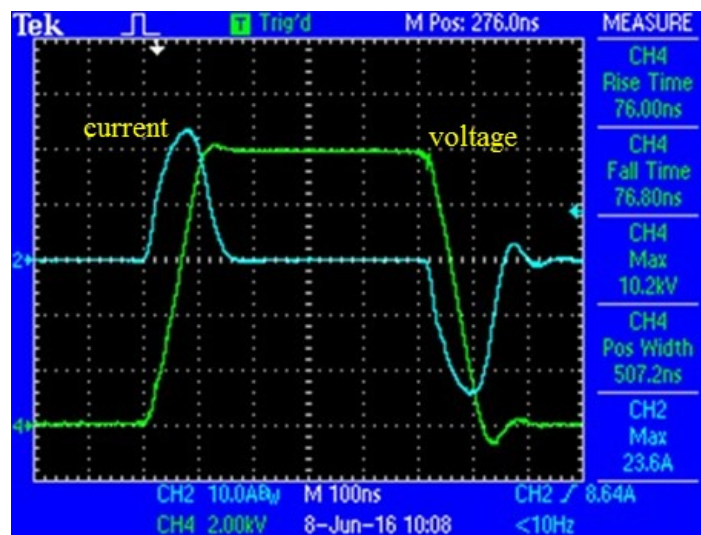

Fig. 31: Measured pulse into a 150 pF load, voltage (green)—2 kV/div, and current (blue)—10 A/div, 100 ns/div [106].

5.9.2.3.2   CERN PS KFA45

As mentioned in section 5.9.2.2.4, the CERN PS KFA45 kicker system is a 45-year-old PFL based system and it is becoming very challenging to find a commercial replacement for the 80 kV SF6 gas filled coaxial PFL cables. Hence, it would be highly advantageous to replace both the PFL and thyratron by a semiconductor based pulse generator, e.g., an IA or a Marx generator.

The specifications of the output pulse from the pulse generator are 40 kV, 3 µs flat-top duration, 30 ns rise and fall times, and 1 Hz repetition rate: it is proposed that the output of the magnet would be terminated in a short circuit and, hence, the load current would be 3.2 kA. The rise and fall time specifications are particularly challenging. A theoretical study for a Marx generator topology, using approximately 50 stages, of 800 V per stage, has commenced; each stage would consist of 24 SiC MOSFETs in parallel. Each MOSFET would conduct approximately 140 A pulses. A 4-stage prototype has been designed and tested, with almost full current at 3 kV output pulse voltage: this prototype allows the proposed design to be evaluated, in order to assess the technological advantages of such a system and limitations for the scale up to full voltage [107].

A Marx stage consists of 24 SiC MOSFETs in parallel, arranged in eight so-called 'switch units' of three MOSFETs per switch unit. A 60 µF capacitance is associated with each switch unit, giving 480 µF per stage. The capacitor bank associated with each switch unit comprises two parallel 30 µF capacitors: this parallel arrangement decreases the series inductance and increases the total current carrying capability. Hence, there are sixteen capacitors in total per stage.
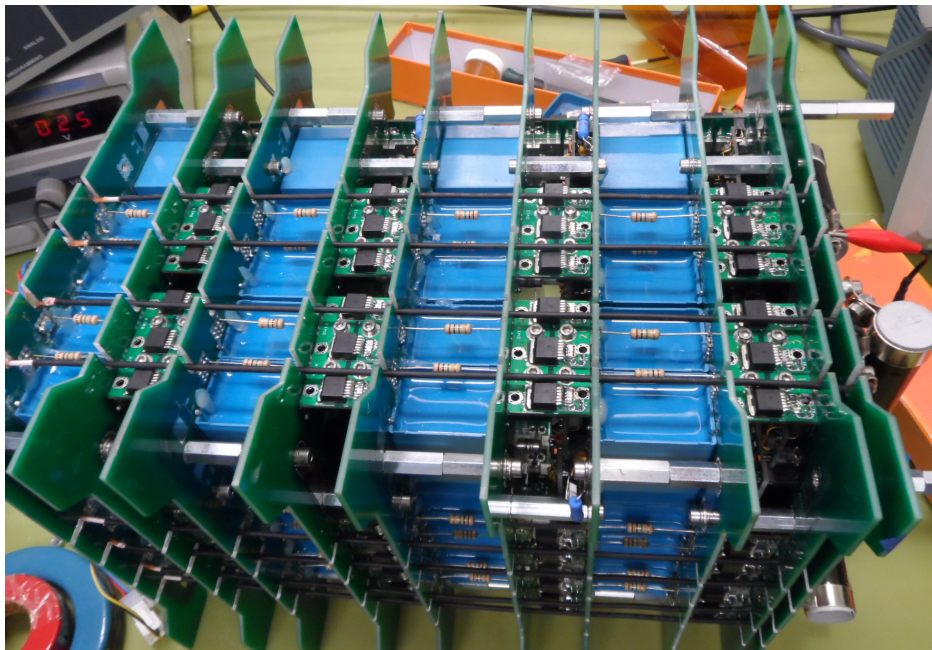
Fig. 32: Four Marx stages: four return conductors per side

The four stages of the Marx generator are assembled in a coaxial type structure, as shown in Fig. 32, in order to limit the loop inductance. The current flows to the load through the MOSFETs and capacitors, placed around the sides of this structure, and returns back through external wires, four per side. A four stage Marx generator was tested to obtain a load current pulse of 2.7 kA, and 3.2 kV, into a 1.18 Ω resistive load: the measured load voltage pulse is shown in Fig. 33. The measured rise and fall times, 10% to 90%, were both ~50 ns. The measured droop is ~1.6% during the 1.5 µs flat top: the expected droop during this period, estimated from an effective capacitance of 120 µF and 1.18 Ω load resistance, is 1.1%.
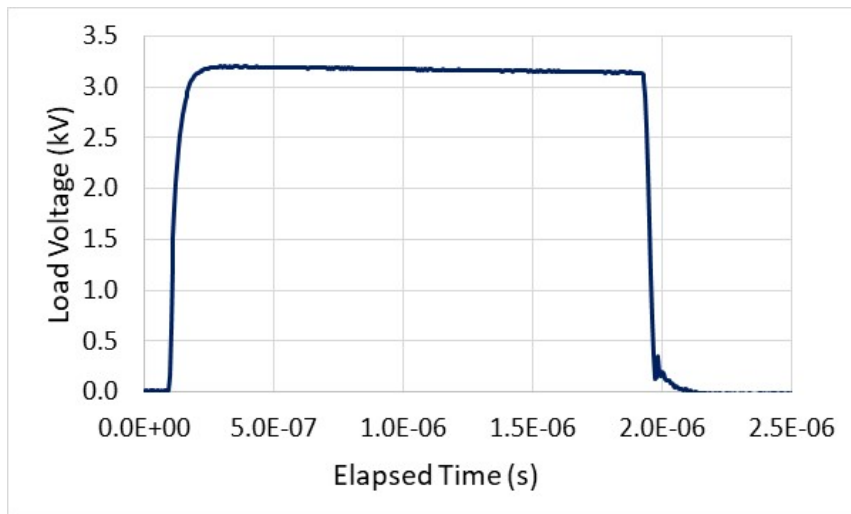
Fig. 33: Measured load voltage pulse for four Marx stages (pre-charge = 800 V/stage)

Although, the initial measurements and test results are promising, there are ongoing tests to determine whether the Marx generator is a good candidate for high current pulsed power generators for kicker magnet applications. In addition, the scaling up of this concept has many complexities including the separation between the main circuit and wires carrying the return current [107]. Furthermore modifications of the Marx generator are under consideration so that it can operate with a kicker magnet terminated in a short circuit. Future tests will include long-term stability and reliability.

5.9.2.4 Series switch topology

The simplest solid-state modulator topology consists of a capacitor bank and a stack of solid-state switches connected in series. The modulator can also be connected to the load with a step-up transformer. Figure 34 shows a simplified schematic of a series switch modulator topology. The advantages of the series switch topology are that it is relatively simple and it can be used to generate both short and long pulses. If there is not an output transformer, the maximum pulse length is a function of the value of the capacitor bank, the load impedance, and the acceptable droop [89].
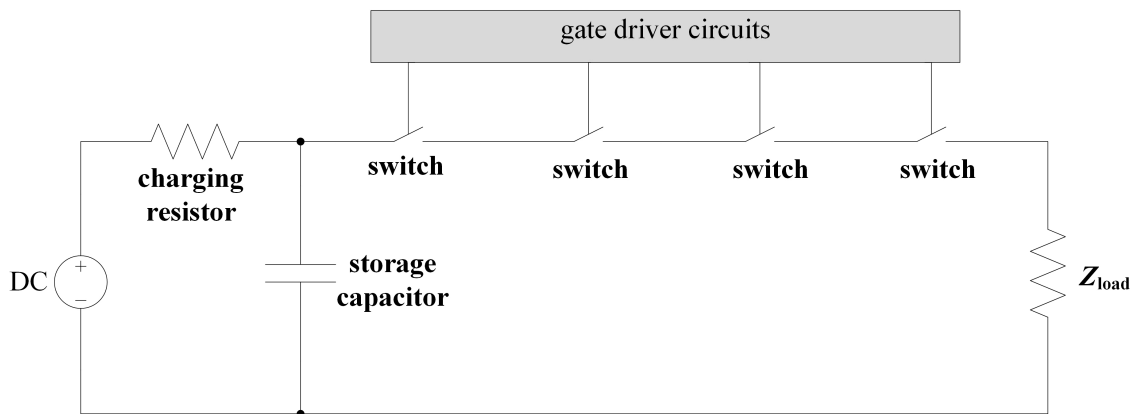
Fig. 34: Simplified schematic of a series switch topology [89]

The disadvantages of the series switch topology include the fact that the gate drive circuit of the power switches are electrically floating and not referenced to the ground: this requires use of transformers or fibre optics between any ground referenced control circuits and the gate driver for the power semiconductor switches. The timing of the trigger pulses has to be well synchronised at the gates

of the power switches to keep the voltage stress over the switches to an acceptable level. Special care must be taken in designing the fibre optic link for the trigger signals, in order to avoid time jitter between the stacked switches [108]. In addition, if a single switch in the stack fails, the voltage stress over other switches is increased and this may cause the other switches to fail, unless appropriate redundancy is included.

A pulse power modulator developed at Saskatchewan Accelerator Laboratory generated up to 20 kV pulses with 10 A of load current. The flat-top length could be adjusted from 0.5 µs to 6 µs, the repetition rate was up to 360 Hz and the rise and fall times were 100 ns and 1 µs, respectively [109]. A bipolar pulse modulator was developed at TRIUMF. This modulator generated ±15 kV pulses with adjustable pulse length from 25 ns to 120 ns. The rise and fall times were less than 32 ns, from 10% to 90% of the pulse voltage, and the repetition rate was fixed at 930 kHz. To achieve these specifications the pulses were reflected back and forth on a low loss coaxial cable [110].

A pulse power modulator designed for a kicker for the ISAC facility at TRIUMF generated unipolar −3.5 kV pulses with a repetition rate up to 52 kHz. The pulse width was adjustable from 350 ns to longer than 10 s and the rise and fall times were 63 ns, from 10% to 90%. To achieve pulse durations of up to 10 s a novel gate driver circuit was developed [111].

A MOSFET stack based pulse modulator for muon lifetime measurements at Paul Scherrer Institute, Switzerland, generated pulses up to ±12.5 kV for deflector plates of a kicker system. The load consisted of deflector plates, the capacitance of which was in total 108 pF. The length of the pulse flat top was adjustable from 200 ns as a minimum, and the rise and fall times less than 40 ns from 10% to 90% of the pulse voltage. The repetition rate was up to 77 kHz [108, 112].

A pulse power modulator operating at over 2 MHz repetition rate and based on stacked switch technology was developed in Extreme Energy Density Institute at Nagaoka University of Technology in Japan. This modulator delivers 5 kV pulses to a 70 Ω load. The peak current was 75 A, operation frequency up to 2.1 MHz, rise and fall times of 33 ns and 43 ns, respectively, and the pulse width of the load voltage was 240 ns [113].

A series switch modulator based on MOSFET switches has also been built to generate very short pulses. An example is a prototype pulse modulator for the damping ring kicker of the ILC. This pulse modulator produced 4.8 kV pulses with a pulse width of 14 ns and with rise and fall times close to 5 ns. In order to achieve the specifications for pulse width, the MOSFET stack was designed to be its own PFL [114].

5.10 Striplines

The CLIC study is exploring the scheme for an electron−positron collider with high luminosity and a nominal centre-of-mass energy of 3 TeV. The CLIC pre-damping rings and damping rings (DR) will produce, through synchrotron radiation, ultra-low emittance beam with high bunch charge, necessary for the luminosity performance of the collider. The role of the DRs is to provide the final stage of damping to the required low emittance beam, at a repetition rate of 50 Hz. The normalized emittance requirements are extremely low, 500 nm in the horizontal plane and 5 nm in the vertical plane. Once the beam is damped to the final emittance values, it is extracted from the DRs and injected into the booster linac, where the beam will be accelerated from 2.86 GeV to 9 GeV. Hence, the extraction system from the CLIC DR must not result in blow up of the beam emittance: any ripple or droop on the extraction kicker pulse will produce beam size jitter which could be propagated up to the interaction point of the collider. The CLIC DR have strict requirements for low beam-coupling impedance [85]: hence, stripline technology is an excellent choice [115−117].

Important challenges for the CLIC DR kickers are [116, 117]:

(i)   excellent field homogeneity, with only ±0.01% of inhomogeneity allowed over 1 mm radius, in the centre of the aperture;

(ii)   good power transmission, with extremely low ripple, by achieving good impedance matching of the striplines in the deflecting (odd) mode;

(iii)   very low beam-coupling impedance, which should be below 0.05 Ω/turn in the longitudinal plane and 200 kΩ/m in the transverse plane: the beam-coupling impedance is important during the non-deflecting (even) mode.

Injection and extraction stripline kickers are used for fast injection/extraction applications, such as bunch-by-bunch manipulation, with a field rise time of a few ns. This is the case for the tapered striplines designed for the injection upgrade of the Φ factory DAΦNE [57], as well as the kicker system proposed for the ILC DR beam extraction [118]. For the CLIC DR extraction kicker, the curved and tapered electrodes used in DAΦNE would give higher field inhomogeneity than is permissible. Hence, a novel electrode shape has been developed for the CLIC DR extraction kickers that has allowed to achieve the excellent field homogeneity, good matching of both odd and even mode characteristic impedances, and a decrease in the beam-coupling impedance at low frequencies. These studies were carried out by using *HFSS* [21] and *CST* simulation codes [22].

The striplines have both an odd and an even mode impedance: the odd mode is when both electrodes are driven to opposite polarity voltages, to extract beam from the CLIC DR, whereas the even mode is when the electrodes are not driven by pulse generators. The characteristic impedance of both odd and even modes should ideally be optimized to 50 Ω. However, for coupled electrodes this is not possible to achieve. The difference between the even mode and odd mode characteristic impedances is due to the capacitance between the electrodes (C_{12}), and an infinite separation between the electrodes would be needed to uncouple the electrodes, i.e., to ensure that $C_{12} = 0$. Since the beam-coupling impedance is proportional to the even mode characteristic impedance, the even mode impedance is optimized to be 50 Ω. Nevertheless, it is desirable that the odd mode impedance is as close to 50 Ω as possible, to be able to match their impedance to that of commercially available coaxial cables.

Various shapes of electrodes were studied and optimized for beam-coupling impedance, odd mode impedance as close to the even mode impedance as possible, and excellent field homogeneity. In addition the electrode supports, feedthroughs, and manufacturing tolerances were studied. A novel shape of electrode, called a half-moon electrode, was selected as the optimum shape [117].
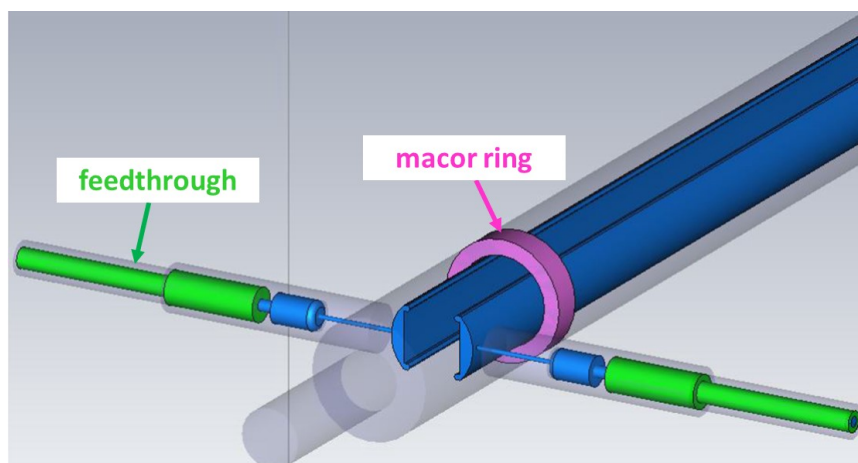
Fig. 35: *CST* model used to optimize the supports and the feedthroughs for the half-moon electrodes

For the optimized half-moon electrode shape, the odd mode characteristic impedance is 40.9 Ω. Since the inductive adder will be connected to each electrode with commercial coaxial cable of 50 Ω impedance, and each electrode will be terminated with 50 Ω (Z_L in Fig. 36), there is an impedance mismatch for the odd mode at both the input and output of the electrodes: impedance mismatches can increase the settling time of the pulse [117]. A new idea was proposed to match the load side characteristic impedance for both the odd and even modes of excitation of the striplines: this is achieved by adding resistor Z_m, shown in Fig**. 36.**

Simulations with *Opera2D* show that the internal inductance of the electrodes, of a stripline kicker, is frequency dependent: at frequencies approaching DC the current is uniformly distributed in each electrode, and the magnetic field can pass through the electrode. Whereas at high frequencies the current distribution is determined by the skin effect and proximity effect: for the CLIC DR striplines the highest current density is on the electrode surface closest to the beam pipe. At high frequencies, the magnetic field hardly penetrates into the electrodes and thus the internal inductance of the electrodes is negligible. Hence, the characteristic impedance of the electrodes is frequency dependent (Fig. 37) [86].
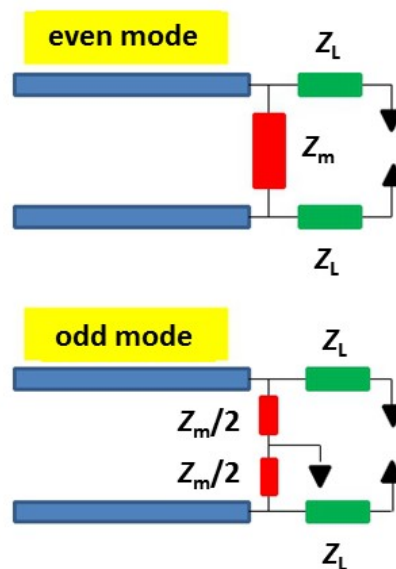

Fig. 36: Proposed method for matching the characteristic impedance for both odd and even modes: adding matching Z_m resistor allows for a tuning of the odd mode characteristic impedance while the even mode characteristic impedance is unchanged [117].

The electric field contribution to the deflection angle is constant at 0.75 mrad (taken from an electrostatic simulation), whereas the magnetic field contribution decreases from a value slightly larger than 0.76 mrad at 50 Hz, to a value of approximately 0.6 mrad, at higher frequencies (Fig. 38): the shape of the magnetic deflection curve, versus frequency, is similar to the shape of the curve shown in Fig. 37 [86].

The maximum field inhomogeneity allowed is ±0.01%, over 1 mm radius, although a radius of 0.5 mm has also been accepted from beam optics considerations [119]. The magnetic field uniformity for different frequencies, for the optimized stripline geometry [117], has been studied with *Opera2D*, and the results are shown in Fig. 39, for radii of 1 mm and 0.5 mm. When considering 1 mm radius, the field uniformity requirement is achieved for frequencies above ~500 kHz. If the good field region is reduced to 0.5 mm radius, the field uniformity requirement is achieved above 10 kHz [86].
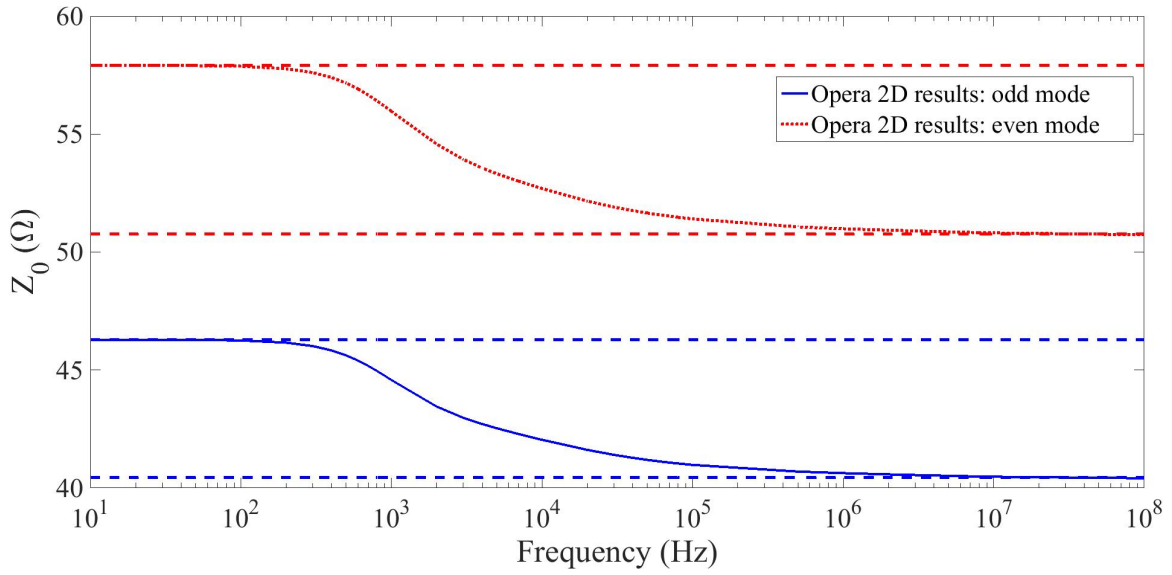
Fig. 37: Odd (blue) and even (red) mode characteristic impedances versus frequency. The dashed lines show the upper and lower values [86].
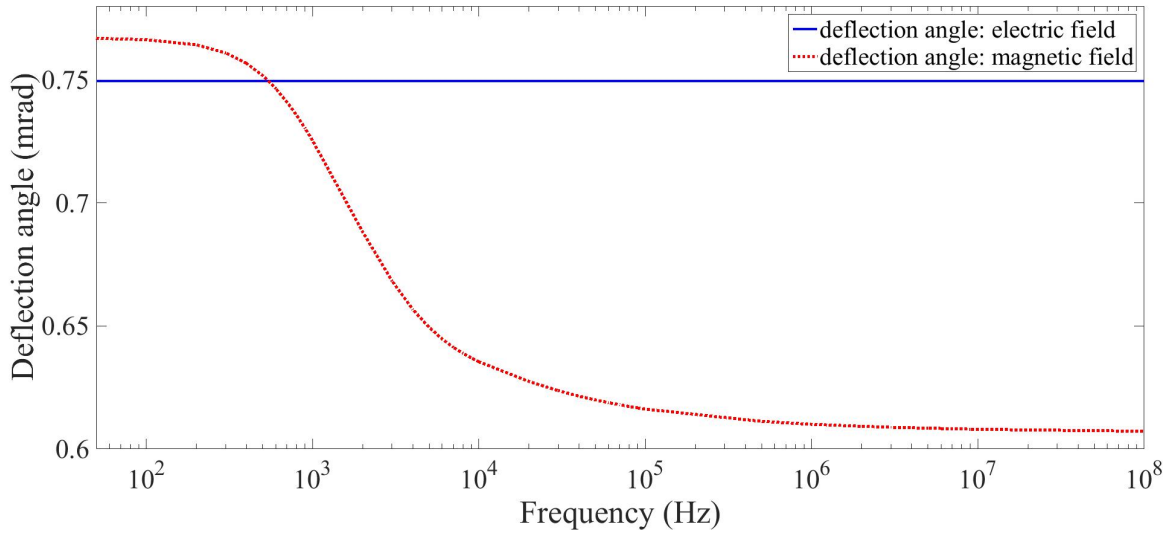

Fig. 38: Deflection angle resulting from the predicted electric and magnetic fields versus frequency, for the optimum (half-moon) geometry of the electrodes of the striplines (±12.5 kV, ±250 A) [86].
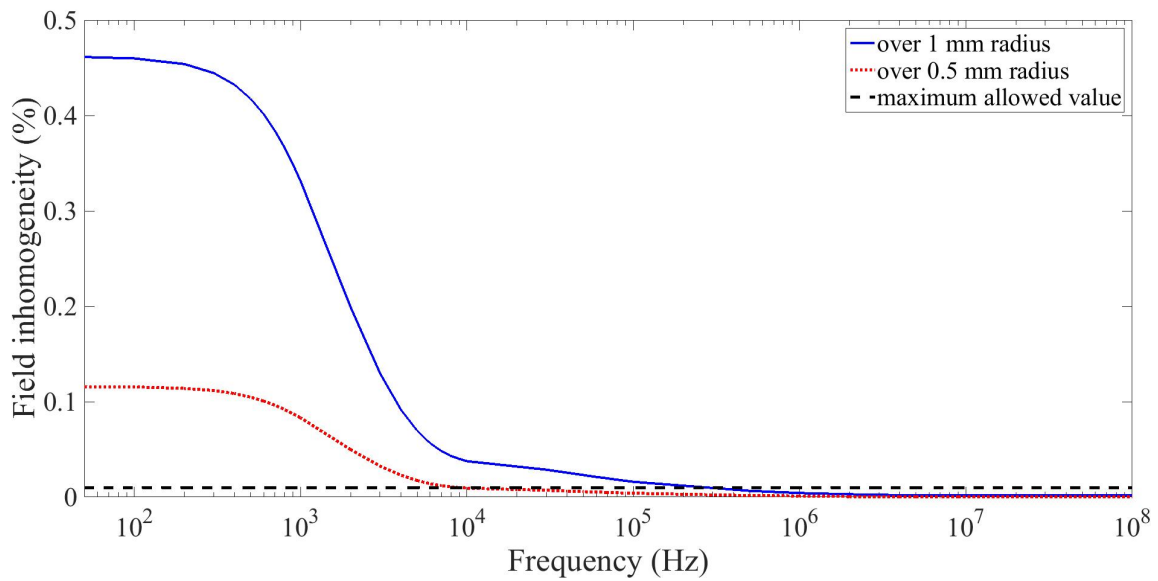
Fig. 39: Magnetic field inhomogeneity versus frequency, over 1 mm radius (blue) and 0.5 mm radius (red). The maximum allowed inhomogeneity, ±0.01%, is shown in black [86].

In order to achieve the required deflection angle of 0.75 mrad for the magnetic field, for the CLIC DR, given the relatively high-frequency content of a pulse, the odd mode characteristic impedance of the striplines must be matched by the termination resistance. It is possible to match the even mode impedance to 50 Ω and the odd mode impedance to 40.9 Ω, by connecting a resistance (Z_m) of 450 Ω between the output of the two electrodes, as shown in Fig. 36. However the output current to be supplied by the IA (see section 5.9.2.2.1) will be increased from 250 A to ~310 A.
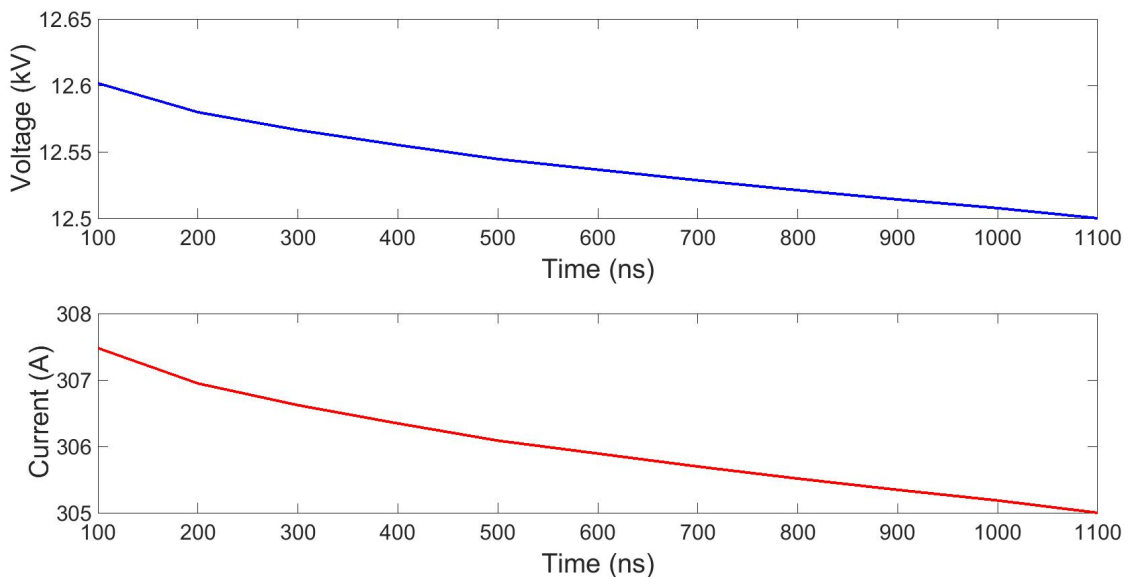
Fig. 40: Modulation of the flat-top voltage (top) and current (bottom), in order to obtain a 'constant' deflecting field (40.9 Ω termination).

As a result of the frequency dependence of the impedance and hence deflection angle of the striplines, and given the frequency content of the current and voltage waveform used to excite the striplines, in order to achieve a deflection angle flat to within ±0.02%, the 'flat top' of the required

excitation waveforms is not exactly flat, as shown in Fig. 40 [120]. It has been demonstrated that the prototype IA, developed for the CLIC DRs, can generate the required shape of the output waveform [92].

The prototype striplines have been installed at ALBA Cells, Spain, initially for beam impedance and DC field homogeneity measurements: these measurements will be carefully compared to predictions from simulations. Following the assembly and laboratory testing of the 12.5 kV prototype inductive adders, these may also be installed at ALBA for testing together with the striplines.

5.11 Double kicker system

A double kicker system (Fig. 41), consisting of two 'identical' ferrite loaded kicker magnets and a single power supply, has been developed at KEK [121, 122]. The first kicker extracts the beam from a damping ring and the second kicker, displaced from the first kicker by a suitable Betatron phase, results in anti-phase ripple to that of the first kicker (Fig. 42).
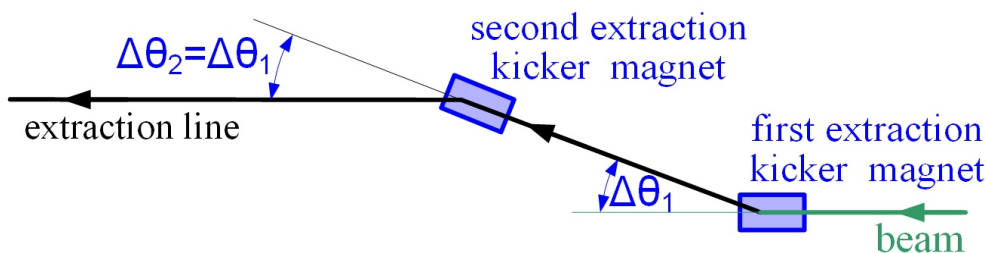

Fig. 41: First and second kickers separated by a betatron phase of $2n\pi$: for a betatron phase of $(2n-1)\pi$ the second kick would be towards the vertical direction.
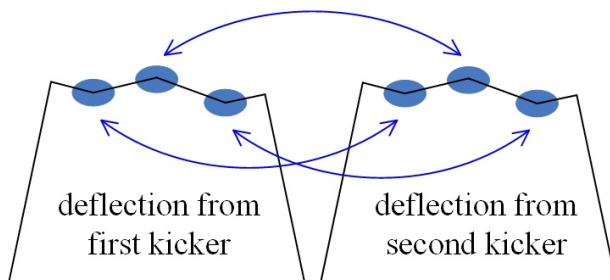

Fig. 42: Exactly the same flat top ripple from both kickers ideally results in ripple cancellation

Theoretically, using a double kicker system, the effect of ripple in the two kickers and small variations in the output of the HVDC supplies can completely cancel. In addition, theoretically, the double kicker can compensate for some field inhomogeneity in each kicker; this therefore permits the field uniformity requirement of an individual kicker to be relaxed, while still achieving excellent overall effective deflection uniformity. However, this places demanding requirements on the beam optics.

Measurements were carried out at the KEK/ATF with a double kicker system: the two kicker magnets were nominally identical, ferrite loaded, transmission-line magnets. However, to reduce beam-coupling impedance, the inside of the ceramic tube in the magnet apertures was coated with 1 μm thick titanium nitride (TiN): the thickness of the TiN coating is probably not uniform. This is evidenced by the fact that the second kicker had an apparent deflection angle of only 83% of the first kicker (for approximately the same current flow [121]): the deflection angle was determined from measurements of the beam orbit, shot by shot, in the extraction line [121]. The two KEK kickers each had 25 cells and were manufactured to high mechanical accuracy. In addition, the ferrite used (TDK-PE14) was from a single manufactured batch [123]: thus magnetically the two kickers should perform in a very similar manner.

The phase advance of the two kickers, although nominally π, was experimentally determined to minimise the jitter angle in the two kicker mode. Subsequently, to measure the equivalent jitter in single kicker mode, the second kicker was replaced with a dipole [122]: the strength of the dipole was adjusted to give the same average beam trajectory as for the double kicker. The dipole had a small aperture and a high stability power supply, thus its field uniformity and field stability was very good. All measurements were made with single bunches, i.e., at a particular time on the kick field waveform [122].

BPMs were used to determine the ripple of the double kicker system. The ATF damping ring had button BPMs with a positional resolution of between 20 μm and 30 μm. The extraction line used both Cavity BPMs (2 μm resolution) and stripline BPMs (20 μm to 30 μm resolution). The KEK double kicker achieved a factor of ~3.3 reduction in kick jitter angle, with respect to a single kicker [122]. The resolution of the BPMs limited the optimization of the phase advance and thus the jitter angle reduction.

5.12 Ultra-fast kickers

Ultra-fast kicker systems generally use either fast high-voltage MOSFETs [108, 124−127] or a Fast Ionization Dynistor (FID) [129–131] or a drift-step recovery diode [132]: the FID is also sometimes called a fast ionization device. Turn on of a thyristor by impact ionization is also an interesting means of achieving super-fast turn-on of a thyristor [133]. Where sub-nanosecond jitter is required, only semiconductor switches can be used. A case in point is the tail-clipper kicker for the CLIC Test Facility 3 (CTF3) [134] at CERN: the tail clipper must have a fast field rise time, of 5 ns or less, to minimize uncontrolled beam loss. For this application, there are eight identical pulse generators: each pulse generator is composed of a 50 Ω PFL, a fast semiconductor MOSFET switch, 50 Ω stripline electrodes (no magnetic material) and a matched terminating resistor [127, 128]. The deflection of the electron beam makes use of both the electric and magnetic field in the stripline electrodes: in order that the effects of the electric and magnetic field do not cancel, the striplines are fed from the beam exit end of the plates (Fig. 43).
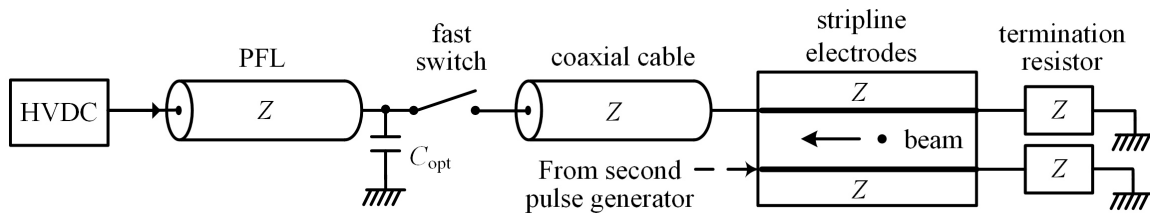
Fig. 43: Simplified schematic of CTF3 tail-clipper kicker

The overall length of the stripline assembly is mechanically sub-divided into four striplines of equal length of 380 mm each: a pair of stripline electrodes is energized a time delay of 1.27 ns (0.38 m/c) after the previous stripline electrodes to minimize the overall apparent rise time of the kick [127]. Each set of striplines is driven by two fast switches, one connected to a positively charged PFL and the other connected to a negatively charged PFL (Fig. 43). Figure 44 shows a pulse, measured using a fast current transformer, flowing in the load, and generated using a MOSFET switch: the 56 A of current has a 10% to 90% rise time of 2.5 ns. A novel design of gate driver results in an overall 3-sigma jitter of less than ±300 ps for the modulator system [127].

A FID was considered for use for the CTF3 tail clipper but a suitable device was not delivered in time.

Fig. 44: Measured trigger pulse (cyan trace – 1 V/div), gate driver output (green trace – 2 V/div), and load current (lilac trace – 10 A/div) for a CTF3 tail-clipper kicker system.

5.13 Resistive terminators

In order that the impedance of the resistive terminator is matched to the system impedance, over a wide range of frequencies, high-power resistor disks are generally used, which are housed in a coaxial structure to minimize inductance of the terminator. The coaxial housing is normally tapered, with the maximum internal diameter of housing at the input end [135]: this design permits the resistive terminator to withstand a high pulse voltage while minimizing the parasitic inductance of the terminator.

Current distribution within the resistor discs, during the pulse, is dependent upon the resistivity of the disks and the frequency content of the pulse. As a result of proximity effect, image current flows on the inside diameter of the coaxial housing. For cooling and insulation purposes, the terminator is generally filled with oil [18]. Long-term stability of the resistance value is linked to the ageing of the resistor discs: the ageing process is affected by the oil [68]. In order to accelerate the stabilization towards a final value of resistance, the discs are pre-impregnated under vacuum at high temperature. The short-term stability is linked to the temperature coefficient of the resistor material. Each current pulse will raise the temperature of the resistor stack: thus, where high stability is required, a suitable heat exchanger is required to maintain the oil temperature.

The resistor discs also exhibit a voltage coefficient of resistance, which is typically around −1.5%/kV/cm: thus the resistive terminator changes in value during the pulse. For high-precision applications, where a well-matched system is required, the voltage dependence of the terminator must be taken into account at the design stage.

5.14 **Acknowledgements**

There are many people who have given invaluable help and contributed to the preparation of the CAS lectures, and to whom I am very grateful. These include C. Belver Aguilar, A. Chmielinska, L. Ducimetière, T. Fowler, J. Holma, T. Kramer, L. Redondo, B. Salvant, V. Senaj, L. Sermeus, T. Stadlbauer, L. Vega Cid, V. Vlachodimitropoulos, and D. Woog. I thank all of these colleagues for their contributions, and apologize to anyone who I forgot to mention.

References

[1] G.H. Rees, in Proceedings of the CAS-CERN Accelerator School, 5th General Accelerator Physics Course, Jyväskylä, Finland, 7-18 September 1992, CERN 94-01 v 2, (CERN, Geneva, 1994), pp. 346-355, https://doi.org/10.5170/CERN-1994-001.

[2] C. Bovet, R. Gouiran, I. Gumowski and K.H. Reich, A selection of formulae and data useful for the design of A.G. synchrotrons, CERN/MPSSI/Int. DL/70/4.

[3] D. Fiander, K.D. Metzmacher and P.D. Pearce, Kickers and septa at the PS complex, CERN, Proc. KAON PDS Magnet Design Workshop, Vancouver, Canada, 3−5 October 1988, pp. 71−79.

[4] M.J. Barnes and G.D. Wait, Low power measurements on an AGS injection kicker magnet, Proc. 22nd Particle Accelerator Conference (PAC'07), Albuquerque, New Mexico, USA, 25−29 June 2007, pp. 2188–2190, https://doi.org/10.1109/PAC.2007.4441192.

[5] L. Ducimetière, Advances of transmission line kicker magnets, Proc. 21st Particle Accelerator Conference (PAC'05), Knoxville, USA, 16−20 May 2005, pp. 235–239, https://doi.org/10.1109/PAC.2005.1590404.

[6] J.N. Weaver *et al.*, Design, analysis and measurement of very fast kicker magnets at SLAC, Proc. 13th Particle Accelerator Conference (PAC'89), Chicago, USA, 20−23 March 1989, pp. 411–413, https://doi.org/10.1109/PAC.1989.73062.

[7] W. Zhang *et al.*, An overview of high voltage dielectric material for travelling wave kicker magnet application, Proc. 25th International Power Modulator Conference and High Voltage Workshop, Hollywood, California, USA, 30 June–3 July 2002, pp. 674–678.

[8] M.J. Barnes, G.D. Wait and I.M. Wilson, Comparison of field quality in lumped inductance versus transmission line kicker magnet, Proc. 4th European Particle Accelerator Conference (EPAC'94), London, UK, 27 June–1 July 1994, pp. 2547–2549.

[9] L. Ducimetière, N. Garrel, M.J. Barnes and G.D. Wait, The LHC injection kicker magnet, Proc. 20th Particle Accelerator Conference (PAC'03), Portland, Oregon, USA, 12−16 May 2003, pp. 1162–1164, https://doi.org/10.1109/PAC.2003.1289639.

[10] D.C. Fiander, K.D. Metzmacher and L. Sermeus, AA ejection kicker for AA Complex, CERN PS/BT/Note 87-22.

[11] K.D. Metzmacher, L. Sermeus, AA injection kicker for AA Complex, CERN PS/BT/Note 87-5.

[12] M.J. Barnes, F. Caspers, T. Kroyer, E. Metral, F. Roncarolo and B. Salvant, Measurement of longitudinal and transverse impedance of kicker magnets using the coaxial wire method, Proc. 23rd Particle Accelerator Conference (PAC'09), Vancouver, Canada, 4−8 May 2009, pp. 1726−1728.

[13] M.J. Barnes and G.D. Wait, Comparison of measured and predicted inductance per cell for a travelling wave kicker magnet, Proc. 5th European Particle Accelerator Conference (EPAC'96), Sitges, 10−14 Spain, June 1996, pp. 2588–2590.

[14] R.B. Armenta *et al.*, Design concept for AGS injection kicker upgrade to 2 GeV, Proc. 21st Particle Accelerator Conference (PAC'05), Tennessee, USA, 16−20 May 2005, pp. 1380–1382, https://doi.org/10.1109/PAC.2005.1590768.

[15] R.B. Armenta *et al*., Electromagnetic modeling of the AGS A10 injection kicker magnet, *IEEE Trans. Appl. Supercond*.,**16** (2006), pp. 293–296, https://doi.org/10.1109/TASC.2005.864458.

[16] Cobham Technical Services, 24 Bankside Kidlington, Oxford OX5 1JE, UK, www.vectorfields.com, accessed 22 December 2017.

[17] M.J. Barnes *et al*., The beam screen for the LHC injection kicker magnets, Proc. 10th European Particle Accelerator Conference (EPAC'06), Edinburgh, Scotland, 26–30 June 2006, pp. 1508–1510.

[18] L. Ducimetière, U. Jansson, G.H. Schröder, E.B. Vossenberg, M.J. Barnes and G.D. Wait, Design of the injection kicker magnet system for CERN's 14TeV proton collider LHC, Proc. 10th International Pulsed Power Conference, Albuquerque, New Mexico, USA, 10–13 July 1995, pp. 1406–1411.

[19] M.J. Barnes, G.D. Wait and L. Ducimetière, Inductance calculations and measurements for the CERN LHC injection pulse forming network, Proc. 7th European Particle Accelerator Conference (EPAC'00), Vienna, Austria, 26–30 June 2000, pp. 2355–2357.

[20] Integrated Engineering Software, Winnipeg, Manitoba, Canada, www.integratedsoft.com, accessed 22 December 2017.

[21] ANSYS, http://www.ansys.com/, accessed 22 December 2017.

[22] CST - Computer Simulation Technology, http://www.cst.com, accessed 22 December 2017.

[23] T. Kroyer, F. Caspers and E. Gaxiola, Longitudinal and transverse wire measurements for the evaluation of impedance reduction measures on the MKE extraction kickers, CERN AB-Note-2007-028.

[24] F. Caspers *et al*., The fast extraction kicker system in SPS LSS6, Proc. 10th European Particle Accelerator Conference (EPAC'06), Edinburgh, Scotland, 26–30 June 2006, pp. 3125–3127.

[25] C. Zannini, Electromagnetic simulation of CERN accelerator components and experimental applications, PhD Thesis, École Polytechnique Fédérale de Lausanne, CERN-THESIS-2013-076 (available on-line).

[26] H. Day, PhD thesis, University of Manchester, 2019, CERN-THESIS-2013-083 (available on-line).

[27] M. Beck, Master thesis, Karlsruhe Institute of Technology, Germany, 2015, CERN-THESIS-2015-374 (available on-line).

[28] Y.H. Chin, K. Takata, T. Toyama, Y. Shobuda and J. Kamiya, Impedance and beam instability issues at J-PARC Rings, Proceedings of HB2008, Nashville, Tennessee, USA, 2008.

[29] J. Uythoven *et al*., Beam induced heating of the SPS fast pulsed magnets, Proc. 9th European Particle Accelerator Conference (EPAC'04), Lucerne, Switzerland, 5–9 July 2004, pp. 623–625.

[30] J. Rümmler, DESY, DESY III dump system with one fast kicker, Proc. 16th Particle Accelerator Conference (PAC'95), Dallas, Texas, USA, 1–5 May 1995, pp. 1933–1935, https://doi.org/10.1109/PAC.1995.505411.

[31] B. Salvant *et al*., Beam induced RF heating in LHC in 2015, Proc. 7th International Particle Accelerator Conf. (IPAC'16), Busan, Korea, 8−13 May 2016, pp. 602−605.

[32] M.J. Barnes *et al*., Beam induced ferrite heating of the LHC injection kickers and proposals for improved cooling, Proc. 4th International Particle Accelerator Conf. (IPAC'13), Shanghai, 12−17 May 2013, pp. 732−734.

[33] W. Zhang, L.A. Ahrens, J. Glenn, J. Sandberg and N. Tsoupas, Beam coupling phenomena in fast kicker systems, Proc. 19th Particle Accelerator Conference (PAC'01), Chicago, USA, 18–22 June 2001, pp. 3708–3710, https://doi.org/10.1109/PAC.2001.988227.

[34] H. Tsutsui, Some simplified models of ferrite kicker magnet for calculation of longitudinal coupling impedance, CERN-SL 2000-004 AP, 2000.

[35] G. Nassibian, CERN/PS 84-25 (BR), 1984; CERN/PS 85-68 (BR), 1986.

[36] Y. Shobuda, Y. Irie and T. Toyama, Analytical approach to evaluate coupling impedances of traveling kicker magnets, *Nuclear Instrum. Methods in Phys. Res. A* **691** (2012) 135–151, https://doi.org/10.1016/j.nima.2012.06.066.

[37] N. Biancacci *et al.*, Impedance calculations for simple models of kickers in the non-ultrarelativistic regime, Proc. 2nd International Particle Accelerator Conf. (IPAC'11), San Sebastián, Spain, 4−9 September 2011, pp. 772-774.

[38] F. Caspers, Impedance Determination, in: Handbook of Accelerator Physics and Engineering (World Scientific, 1999).

[39] M.J. Barnes *et al.*, Measurement and analysis of SPS kicker magnet heating and outgassing with different bunch spacing, Proc. 23rd Particle Accelerator Conference (PAC'09), Vancouver, Canada, 4−8 May 2009, pp. 4264−4266.

[40] M.J. Barnes, F. Caspers, L. Ducimetière, N. Garrel and T. Kroyer, An improved beam screen for the LHC injection kickers, Proc. 22nd Particle Accelerator Conference (PAC'07), Albuquerque, New Mexico, USA, 25−29 June 2007, pp. 1574–1576, https://doi.org/10.1109/PAC.2007.4440827.

[41] J. Rümmler, Kicker Types for in- and ejection in the damping rings of TESLA, DESY/MIN December 2000.

[42] F. Caspers, A. Mostacci and H. Tsutsui, Impedance evaluation of the SPS MKE kicker with transition pieces between tank and kicker module, CERNSL-2000-071 (AP).

[43] H. Hahn, A. Dunbar, C.I. Pai, R.T. Sanders, N. Tsoupas and J.E. Tuorzzolo, The RHIC beam abort kicker system, Proc. 18th Particle Accelerator Conference (PAC'99), New York, USA, 29 March–2 April 1999, pp. 1100–1102, https://doi.org/10.1109/PAC.1999.795461.

[44] H.J. Tran, M.J. Barnes, G.D. Wait and Y. Yan, Longitudinal impedance of a prototype kicker magnet system, Proc. 15th Particle Accelerator Conference (PAC'93), Washington, D.C, USA, 17−20 May 1993, pp. 3502−3404, https://doi.org/10.1109/PAC.1993.309664.

[45] P. He, H.C. Hseuh and R.J. Todd, Metallization of ceramic vacuum chambers for SNS ring injection kicker magnets, *Thin Solid Films* **420–421** (2002) 38–42, https://doi.org/10.1016/S0040-6090(02)00661-2.

[46] M. Pont, R. Nunez and E. Huttel, Septum and kicker magnets for the alba booster and storage ring, Proc. 2nd International Particle Accelerator Conf. (IPAC'11), San Sebastián, Spain, 4−9 September 2011, pp.4421−4423.

[47] A.D. Ghodke, D. Angal-Kalinin and G. Singh, Kicker chamber metallization induced effects on the beam in Indus-1, Proc. 2nd Asian Particle Accelerator Conf. (APAC'01), Beijing, China, 17−21 September 2001.

[48] M.J. Barnes, T. Fowler, M.G. Atanasov, T. Kramer and T. Stadlbauer, Effect of a metallized chamber upon the field response of a kicker magnet: simulation results and analytical calculations, Proc. 3rd International Particle Accelerator Conf. (IPAC'12), New Orleans, USA, 20−25 May 2012, pp. 3686−3688.

[49] A. Adraktas, M.J. Barnes, L. Ducimetière, Influence of conducting serigraphy upon field pulse shape of the SPS extraction kicker systems, Proc. 8th International Particle Accelerator Conf. (IPAC'17), Copenhagen, Denmark, 14−19 May 2017, pp. 3491−3494.

[50] M.J. Barnes *et al.*, Studies of impedance-related improvements of the SPS injection kicker system, Proc. 7th International Particle Accelerator Conf. (IPAC'16), Busan, Korea, 8−13 May 2016, pp. 3611−3614.

[51] Y. Shobuda, Y. Irie, T. Toyama, J. Kamiya and M. Watanabe, Measurement scheme of kicker impedances via beam-induced voltages of coaxial cables, *Nucl. Instrum. Methods Phys. Res. A* **713** (2013) 52–70, https://doi.org/10.1016/j.nima.2013.02.037.

[52] V. Vlachodimitropoulos, M.J. Barnes, L. Ducimetière, L.V. Cid and W. Weterings, Predicted beam induced power deposition in the LHC injection kicker magnets for HL-LHC Type Beams,

Proc. 8th International Particle Accelerator Conf. (IPAC'17), Copenhagen, Denmark, 14−19 May 2017, pp. 3471−3474.

[53] H. Day *et al.*, Evaluation of the beam coupling impedance of new beam screen designs for the LHC injection kicker magnets, Proc. 4th International Particle Accelerator Conference (IPAC13), Shanghai, China, 12−17 May 2013, pp. 1649−1651.

[54] M.J. Barnes *et al.*, High voltage performance of the beam screen of the LHC injection kicker magnets, IPAC'14, Dresden, 15−20 June 2014, pp. 541−543.

[55] M.J. Barnes *et al.*, Operational experience of the upgraded LHC injection Kicker Magnets, Proc. 7th International Particle Accelerator Conf. (IPAC'16), Busan, Korea, 8−13 May 2016, pp. 3623−3266.

[56] H. Day, M.J. Barnes, L. Feliciano, Impedance studies of the LHC injection kicker magnets for HL-LHC, Proc. 6th International Particle Accelerator Conf. (IPAC'15), Virginia, USA, May 3-8, 2015, MOPJE038, pp. 370-373.

[57] D. Alesini, S. Guiducci, F. Marcellini and P. Raimondi, Design, test, and operation of new tapered stripline injection kickers for the e$^+$ e$^-$ collider DAΦNE, *Phys. Rev. ST Accel. Beams.* **13** (2010) 111002, https://doi.org/10.1103/PhysRevSTAB.13.111002.

[58] Z. Sobiech, Master thesis, UTP University of Science and Technology, Faculty of Mechanical Engineering, Bydgoszcz, Poland, 2014.

[59] L. Vega Cid, Master Thesis, Universidad del Pais Vasco, Bilbao, Spain, 2015 (in Spanish).

[60] M. Timmins, A. Bertarelli, J. Uythoven and E. Gaxiola, SPS extraction kicker magnet cooling design, AB-Note-2004-005 BT.

[61] L. Vega *et al.*, Thermal analysis of the LHC injection kicker magnets, *J. Phys. Conf. Ser.*, **874** (2017) 012100, https://doi.org/10.1088/1742-6596/874/1/012100.

[62] M.J. Barnes, L. Ducimetière, N. Garrel, B. Goddard, V. Mertens and W. Weterings, Analysis of ferrite heating of the LHC injection kickers and proposals for future reduction of temperature, Proc. 3rd International Particle Accelerator Conf. (IPAC'12), New Orleans, 21−26 May 21-26, pp. 2038−2040.

[63] M.J. Barnes *et al.*, Operational experience of the upgraded LHC injection kicker magnets during Run 2 and future plans, *J. Phys. Conf. Ser.*, **874** (2017) 012101, https://doi.org/10.1088/1742-6596/874/1/012101.

[64] T.S. Sudarshan and J.D. Cross, The effect of chromium oxide coatings on surface flashover of alumina spacers in vacuum, *IEEE Trans. Electr. Insul.*, **EI-1I** (1976) 32.

[65] T. Shioiri, N. Asari, S. Saito, H. Nakamuta, M. Homma and K. Suzuki, Effect of chromium oxide coating on surface flashover characteristics of ceramic in vacuum, XXIInd Int. Symp. on Discharges and Electrical Insulation in Vacuum-Matsue-2006, pp. 140−143, https://doi.org/10.1109/DEIV.2006.357251.

[66] G. Arduini *et al.*, Performance of the CERN SPS fast extraction for the CNGS facility, Proc. 21st Particle Accelerator Conference (PAC'05), Knoxville, USA, 16−20 May 2005, pp. 1757–1759.

[67] B. Goddard, M. Barnes, L. Ducimetière, W. Höfle and G. Kotzian, Emittance growth at LHC injection from SPS and LHC kicker ripple, Proc. 11th European Particle Accelerator Conference (EPAC'08), Genoa, Italy, 23−27 June 2008, pp. 3629–3631.

[68] M.J. Barnes, G.D. Wait and L. Ducimetière, Low voltage measurements on nine PFNs for the LHC injection kicker systems, Proc. 8th European Particle Accelerator Conference (EPAC'02), Paris, France, 3−8 June 2002, pp. 2520–2522.

[69] E2V Technologies, 'Hydrogen Thyratrons Preamble', https://www.tayloredge.com/reference/Electronics/VacuumTube/thyratron_preamble.pdf, accessed 22 December 2017.

[70] L. Ducimetiere and D.C. Fiander, Commutation losses of a multigap high voltage thyratron, IEEE Conference Record of the 1990 Nineteenth Power Modulator Symposium, San Diego, USA, 26−28 June 1990, pp. 248−253.

[71] R.L. Cassel and T.S. Mattison, Kicker prepulse canceller, IEEE Conference Record of the 1991 Particle Accelerator Conference, 6−9 May 1991, pp. 3162−3164.

[72] M.J. Barnes and G.D. Wait, A mathematical model of a three-gap thyratron simulating turn-on, Proc. 9th International Pulse Power Conf., Albuquerque, USA, 21−23 June 1993, pp. 293−296, https://doi.org/10.1109/PPC.1993.513335.

[73] G.D. Wait, M.J. Barnes, K.D. Metzmacher and L. Sermeus, The application of saturating inductors for improving the performance of the CERN PS kicker systems, Proc. 17th Particle Accelerator Conf. (PAC'97), Vancouver, Canada, 12−16 May 1997, pp. 1328−1330.

[74] M.J. Barnes, G.D. Wait, E. Carlier, L. Ducimetière, G.H. Schröder and E.B. Vossenberg, A fast 60 kV resonant charging power supply for the LHC inflectors, Proc. 17th Particle Accelerator Conference (PAC'97), Vancouver, Canada, 12–16 May 1997, pp. 1325–1327.

[75] M.J. Barnes, G.D. Wait, L. Ducimetière, G.H. Schröder and E.B. Vossenberg, Measurements on a fast 66 kV resonant charging power supply for the LHC inflectors, Proc. 6th European Particle Accelerator Conference (EPAC'98), Stockholm, Sweden, 22–26 June 1998, pp. 2278–2280.

[76] J.A. Uythoven, E.H.R. Gaxiola and M.A. Timmins, Upgrade of the SPS extraction kickers for LHC and CNGS operation, Proc. 8th European Particle Accelerator Conf. (EPAC'02), Paris, France, 3−8 June pp. 2517−2519.

[77] V. Senaj, N. Voumard, M.J. Barnes and L. Ducimetière, Optically isolated circuit for failure detection of a switch in an HV series connected stack, Proc. 17th IEEE International Pulsed Power Conference, Washington DC, USA, 29 June–2 July 2009, https://doi.org/10.1109/PPC.2009.5386389.

[78] C. Boatella Polo, SEE Single Event Effects, ESA-CERN-SCC Workshop, CERN, 09−10 May 2017, https://indico.cern.ch/event/635099/contributions/2570672/attachments/1456364/2249943/Single_Event_Effecs_Radiation_Course_May_2017_SEE_CBP.pdf

[79] H.R. Zeller, Cosmic ray induced failures in high power semiconductor devices, *Microelectron. Reliab.*, **37** (1997) 1711, https://doi.org/10.1016/S0026-2714(97)00146-7.

[80] R. Edwards and J. Woodhouse, Determination of high energy neutron voltage stress margins for high voltage IGBT and diode pairs from two manufacturers using energetic particle induced charge spectroscopy, EPICS, IEEE Xplore, Radiation Effects Data Workshop, 2006 IEEE, 17−21 July 2006, https://doi.org/10.1109/REDW.2006.295488.

[81] E. Normand, J.L. Wert, D.L. Oberg, P.P. Majewski, P. Voss and S.A. Wender, Neutron-induced single event burnout in high voltage electronics, *IEEE Trans. Nucl. Sci.*, **44** (1997) 2358, https://doi.org/10.1109/23.659062.

[82] J. Bonthond, J.H. Dieperink, L. Ducimetière, U. Jansson and E. Vossenberg, Dual branch high voltage pulse generator for the beam extraction of the Large Hadron Collider, Proc. 2002 Power Modulator Symposium, Hollywood, USA, 30 June–3 July 2002, pp. 114–117, https://doi.org/10.1109/MODSYM.2002.1189429.

[83] J. Uythoven *et al.*, Calibration measurements of the LHC beam dumping system extraction kicker magnets, Proc. 10th European Particle Accelerator Conference (EPAC'06), Edinburgh, Scotland, 26–30 Jun 2006, pp. 1520−1522.

[84] M.A. Fraser *et al.*, Considerations on an upgrade possibility of the LHC beam dump kicker system, Proc. 7th International Particle Accelerator Conf. (IPAC'16), Busan, Korea, 8–13 May 2016, pp. 3631−3633.

[85] M. Aicheler (ed.) *et al.*, A multi-TeV linear collider based on CLIC technology: CLIC Conceptual Design Report, CERN-2012-007, https://doi.org/10.5170/CERN-2012-007.

[86] C. Belver-Aguilar, M.J. Barnes and L. Ducimetière, Review on the effects of characteristic impedance mismatching in a stripline kicker, Proc. IPAC'16, Busan, Korea, 8−13 May 2016, pp. 3627−3630.

[87] Y. Papaphilippou *et al.*, Conceptual design of the CLIC damping rings, Proc. IPAC'12, New Orleans, USA, May 2012, pp. 1368−1370.

[88] J. Holma *et al.*, Preliminary design of the pulse generator for the CLIC DR extraction system, Proc. PPC'11, Chicago, USA, 19−23 June 2011, pp. 1353−1358, https://doi.org/10.1109/PPC.2011.6191614.

[89] J. Holma, Ph.D. Thesis, Aalto University publication series, Doctoral Dissertations 196/2015, Helsinki, Finland, 2015. CERN-THESIS-2014-359 (available on-line).

[90] K. Takayama (ed.) and Briggs, R.J. (ed.), Induction Accelerators. Springer, 2011. ISBN: 978-3-642-13916-1.

[91] E.G. Cook *et al.*, Solid-state modulator R&D at LLNL, Int. Workshop on Recent Progress of Induction Accelerators, Tsukuba, Japan, 29−31 October 2002.

[92] J. Holma and M.J. Barnes, Prototype inductive adders with extremely flat-top output pulses for the Compact Linear Collider at CERN, paper submitted to a Special Issue of Transactions on Plasma Science on Pulsed Power Science and Technology, 2018.

[93] M. Kemp, High rep-rate CLIC combiner ring kicker, ALERT 2014 Workshop, IFIC-Valencia, Spain, 5−6 May 2014, https://indico.cern.ch/event/306551/contributions/705065/attachments/583693/803464/20_ALERT2014_Kemp.pdf

[94] D. Woog, M.J. Barnes, L. Ducimetière, J. Holma and T. Kramer, Design of an inductive adder for the FCC injection kicker pulse generator, Proc. 8th International Particle Accelerator Conf. (IPAC'17), Copenhagen, Denmark, 14−19 May 2017, WEPVA024, pp. 3312−3315, https://doi.org/10.1088/1742-6596/874/1/012096.

[95] A. Chmielinska, M.J. Barnes, W. Bartmann, F. Burkart and B. Goddard, Preliminary estimate of beam induced power deposition in a FCC-hh injection kicker magnet, Proc. 8th International Particle Accelerator Conf. (IPAC'17), Copenhagen, Denmark, 14−19 May 2017, pp. 3475−3478.

[96] K.-D. Metzmacher and L. Sermeus, The PS injection kicker KFA45 performance for LHC, PS/PO Note 2002-015, CERN, Geneva, 2002.

[97] M.J. Barnes, L. Ducimetière, J. Holma, T. Kramer and A. Fowler, Inductive adders for replacing thyratron based modulators at CERN, Published in: Power Electronics and Applications (EPE'15 ECCE-Europe), 2015 17th European Conference, 8−10 September 2015.

[98] W.L. Willis, in *Pulse-Voltage Circuits*, 1st ed. Eds. R.E. Dollinger and J.W. Sarjeant (Tab Books Inc., 1989), Chap. 3, ISBN 0-8306-9094-8.

[99] J.A. Casey, F.O. Arntz, M.P.J. Gaudreau and M. Kempes, Solid-State Marx bank modulator for the Next Linear Collider, Pulsed Power Conference, 15−18 June 2003, pp. 641−644, https://doi.org/10.1109/PPC.2003.1277791.

[100] A. Krasnykh, R. Akre, S. Gold and R. Koontz, A Solid-state Marx type modulator for driving a TWT, Power Modulator Symposium, 2000. Conference Record of the 2000 Twenty-Fourth International, Norfolk, VA, USA, 26−29 June 2000.

[101] R. Phillips, M.P.J. Gaudreau, M. Kempkes, K. Ostlund and J. Casey, Affordable, short pulse Marx modulator, IEEE International Vacuum Electronics Conference, 22−24 April 2014, Monterey, CA, pp. 455−456.

[102] S.C. Glidden and H.D. Sanders, Solid state Marx generator, Power Modulator Conference, Arlington, VA, USA, 14−18 May 2006, Arlington, https://doi.org/10.1109/MODSYM.2006.365246.

[103] T. Beukers, C. Burkhart, M. Kemp, R. Larsen, M. Nguyen J. Olsen and T. Tang., P1-Marx modulator for the ILC, IEEE Power Modulator and High Voltage Conference, 23-27 May 2010, pp. 21−22.

[104] M.A. Kemp, A. Benwell, C. Burkhart, D. MacNair and M. Nguyen, The SLAC P2 Marx, IEEE Power Modulator and High Voltage Conference, 2012, pp. 1721−1728.

[105] L.M. Redondo and J. Fernando Silva, *IEEE Trans. Plasma Sci.*, **37** (2009) 1632. https://doi.org/10.1109/TPS.2009.2023221.

[106] L.M. Redondo, A. Kandratsyeu, M.J. Barnes, S. Calatroni and W. Wuensch, Solid-state Marx generator for CLIC breakdown studies, to be published in Proc. 2016 IEEE Power Modulator and High Voltage Conference, San Francisco, CA, USA, 5−9 July 2016, https://doi.org/10.1109/IPMHVC.2016.8012824.

[107] L.M. Redondo, A. Kandratsyeu and M.J. Barnes, Marx generator prototype for kicker magnets based on SiC MOSFETs, IEEE Transactions on Plasma Science, 2018, DOI: 10.1109/TPS.2018.2808194.

[108] M.J. Barnes and G.D. Wait, A 25 kV, 75 kHz, Kicker for measurement of muon lifetime, IEEE Trans. Plasma Sci., **32** (2004) 1932, https://doi.org/10.1109/TPS.2004.835455.

[109] C. Figley and D.A. Stensrud, Stacked FET switch for use in a 20 kV klystron modulator. Digest of Tech. Papers PPC'91, San Diego, CA, USA, 16−19 June 1991, pp. 1001−1004, https://doi.org/10.1109/PPC.1991.733455.

[110] G.D. Wait and M.J. Barnes, Pulse width control at 10^6 Pulses/sec and 15 kV for the KAON factory beam chopper, Proc. 9th International Pulse Power Conf., Albuquerque, USA, 21−23 June 1993, pp. 841−844.

[111] M.J. Barnes and G.D. Wait, A FET based kicker for a charge booster for the TRIUMF ISAC Project, Proc. 13th IEEE International Pulsed Power Conf., Las Vegas, USA, 17−22 June 2001, pp. 1245−1248.

[112] R.B. Armenta, M.J. Barnes and G.D. Wait, Precision 25 kV pulse and RF suppression in a 75 kHz kicker, Proc. 15th IEEE International Pulsed Power Conf., Monterey, USA, 13−17 June 2005, pp. 676−679, https://doi.org/10.1109/PPC.2005.300750.

[113] W. Jiang *et al*., MHz Pulsed Power Generator Using MOSFET. Conf. Rec. Power Modulator Symposium and High Voltage Workshop, Hollywood, CA, USA, 30 June 30−3 July 2002, pp. 599−601, https://doi.org/10.1109/MODSYM.2002.1189550.

[114] M.J. Barnes and G.D. Wait, Design and measurements of a damping ring kicker for the ILC, Proc. 22nd Particle Accelerator Conf. (PAC'07), 25−29 June 2007, pp. 846−848, https://doi.org/10.1109/PAC.2007.4440735.

[115] I. Rodríguez, Calculation methodology and fabrication procedures for particle accelerator strip-line kickers: application to the CTF3 combiner ring extraction kicker and TL2 tail clippers, Ph.D. thesis, Universidad Politécnica de Madrid, 2009.

[116] C. Belver-Aguilar, A. Faus-Golfe, F. Toral and M.J. Barnes, Stripline design for the extraction kicker of compact linear collider damping rings, *Phys. Rev. ST: Accel. Beams* **17** (2014) 071003, https://doi.org/10.1103/PhysRevSTAB.17.071003.

[117] C. Belver-Aguilar, PhD thesis, Universidad de Valencia, Spain, 2015. CERN-THESIS-2015-175 (available on-line).

[118] T. Naito, S. Araki, H. Hayano, K. Kubo, S. Kuroda, N. Terunuma and J. Urakawa, *Phys. Rev. ST Accel. Beams* **14** (2011) 051002, https://doi.org/10.1103/PhysRevSTAB.14.051002.

[119] R. Apsimon *et al*., Optics and protection of the injection and extraction regions of the CLIC damping rings, Proceedings of the 4th International Particle Accelerator Conference, IPAC 2013, MOPWO025, pp. 939−941.

[120] C. Belver-Aguilar and M.J. Barnes, Transient studies of the stripline kicker for beam extraction from CLIC damping rings, International Beam Instrumentation Conference (IBIC), Barcelona, Spain, 11−15 September 2016.

[121] T. Imai *et al*, Double Kicker system in ATF, XX International Linac Conference, Monterey, California, LINAC2000, pp. 77−79.

[122] T. Imai, Thesis, Development of Double Kicker System for Stable Beam Extraction, Dept. of Physics, Tokyo University of Science, September 2002.

[123] T. Naito, KEK, private communication.

[124] M.J. Barnes *et al*., A high frequency MOSFET driver for the TITAN facility at TRIUMF, Proc. 15th IEEE International Pulsed Power Conference, Monterey, USA, 13−17 June 2005, pp. 178−181, https://doi.org/10.1109/PPC.2005.300554.

[125] F. Arntz, M. Gaudreau, M. Kempkes, A. Krasnykh and A. Kardo-Sysoev, A kicker driver for the international linear collider, Proc. 22nd Particle Accelerator Conference (PAC'07), Albuquerque, New Mexico, USA, 25–29 June 2007, pp. 2972–2974, https://doi.org/10.1109/PAC.2007.4440638.

[126] F. Arntz, J. Casey, M. Kempkes, N. Butler and M. Gaudreau, Solid-state high voltage pulse power in the 10-100 nanosecond regime, Proc. 10th European Particle Accelerator Conference (EPAC'06), Edinburgh, Scotland, 26–30 June 2006, pp. 3134–3136.

[127] M.J. Barnes, T. Fowler and G. Ravida, Design, Testing and operation of the modulator for the CTF3 tail clipper kicker, Proc. 23rd Particle Accelerator Conference (PAC'09), Vancouver, Canada, 4−8 May 2009, pp. 1723−1725.

[128] M.J. Barnes, T. Fowler, G. Ravida and A. Ueda, Design of the modulator for the CTF3 tail clipper kicker, Proc. 22nd Particle Accelerator Conference (PAC'07), Albuquerque, New Mexico, USA, 25−29 June 2007, pp. 2185–2187.

[129] A. Wolski, Critical R&D issues for the ILC damping rings and new test facilities, Proc. 22nd Particle Accelerator Conference (PAC'07), Albuquerque, New Mexico, USA, 25–29 June 2007, pp. 1945–1949.

[130] T. Naito *et al*., Development of strip-line kicker system for ILC damping ring, Proc. 22nd Particle Accelerator Conference (PAC'07), Albuquerque, New Mexico, USA, 25–29 June 2007, pp. 2772–2774.

[131] D. Alesini, S. Guiducci, F. Marcellini and P. Raimondi, Fast injection kickers for Daphne collider and ILC damping rings, DAPHNE Technical Note, INFN - LNF, Accelerator Division. Note I-17, 6 June 2006.

[132] A. Krasnykh, Development of a Fast High-Power Pulser and ILC DR Injection/Extraction Kicker, SLAC-WP-077, https://inis.iaea.org/search/search.aspx?orig_q=RN:39104667.

[133] A. Gusev, S. Lyubutin, A. Ponomarev, S. Rukin, B. Slovikovsky, S. Tsyranov, High current and current rise rate thyristor based switches, Proc. 21st International Pulsed Power (PPC), Brighton, England, 18-22 June 2017, DOI: 10.1109/PPC.2017.8291162.

[134] G. Geschonke and A. Ghigo, CTF3 design report, CERN/PS 2002-008 (RF).

[135] M.J. Barnes and G.D. Wait, Optimization of speed-up network component values for the 30 Ω resistively terminated prototype kicker magnet, Proc. 15th Particle Accelerator Conference (PAC'93), Washington DC, USA, 17–20 May 1993, pp. 1330–1332.

Bibliography

Eds. O. Brüning, P. Collier, P. Lebrun, S. Myers, R. Ostojic, J. Poole and P. Proudlock, *LHC Design Report*, volume I, The LHC main ring, Chap. 16, Injection system, http://ab-div.web.cern.ch/ab-div/Publications/LHC-DesignReport.html, CERN, Geneva, 2004, CERN-2004-003.

Eds. O. Brüning, P. Collier, P. Lebrun, S. Myers, R. Ostojic, J. Poole and P. Proudlock, LHC Design Report, volume I, The LHC main ring, Chap. 17, Beam dumping system, http://ab-div.web.cern.ch/ab-div/Publications/LHC-DesignReport.html, CERN, Geneva, 2004, CERN-2004-003.

Eds. M. Benedikt, P. Collier, V. Mertens, J. Poole and K. Schindl, LHC Design Report, volume III, The LHC injector chain, http://ab-div.web.cern.ch/ab-div/Publications/LHC-DesignReport.html, CERN, Geneva, 2004, CERN-2004-003.

P. Smith, *Transient Electronics: Pulsed Circuit Technology* (John Wiley & Sons, 2002), ISBN: 047197773X.

L. Ducimetière and D. Fiander, Commutation losses of a multigap high voltage thyratron, Proc. Power Modulator Symposium, San Diego, USA, 26–28 June 1990, pp. 248–253.

K.D. Metzmacher and L. Sermeus, The PSB injection and recombination kicker systems for LHC, CERNPS/CA/Note 2000-004.

K.D. Metzmacher and L. Sermeus, The PS injection kicker KFA45 performance for LHC, CERNPS/PO/Note 2002-015 (Tech.).

L.I. Donley, J.C. Dooling and G.E. McMichael, Using ferrite as a fast switch for improving rise time of IPNS extraction kicker, Proc. 20th Particle Accelerator Conference (PAC'03), Portland, Oregon, USA, 12–16 May 2003, pp. 1159–1161.

W. Zhang *et al.*, Design, development, and construction of SNS extraction fast kicker system, Proc. 20th Particle Accelerator Conference (PAC'03), Portland, Oregon, USA, 12–16 May 2003, pp. 550–552.

G. Nassibian, Travelling Wave kicker magnets with sharp rise and less overshoot, Proc. 8th Particle Accelerator Conference (PAC'79)*, IEEE Trans. Nucl. Sci.,* **NS-26** pp. (1979) 4018.

M.J. Barnes, G.D. Wait and R. Barnes, Estimation of negative mutual coupling between adjacent cells of a magnetic kicker, TRIUMF Design Note TRI-DN-89-K87.

C. Jensen, B, Hanna and R. Reilly, A fast injection kicker magnet for the Tevatron, Proc. 19th Particle Accelerator Conference (PAC'01), Chicago, USA, 18–22 June 2001, pp. 3720–3722.

T. Kawakubo, E. Nakamura and S. Murasugi, Low beam-coupling impedance kicker magnet system generating a high magnetic field with a fast rise time, Proc. 7th European Particle Accelerator Conference (EPAC'00), Vienna, Austria, 26–30 june 2000, pp. 2246–2248.

P.E. Faugeras, E. Frick, C.G. Harrison, H. Kuhn, V. Rodel, G.H. Schröder, J.P. Zanasco, The SPS fast pulsed magnet systems, Proc. 12th Modulator Symposium, New York, USA, Feb. 4–5, 1976 (CERN-SPS-BT-76-1).

J. Wang, Design and test results of kicker units for the positron accumulator ring at the APS, Proc. 16th Particle Accelerator Conference (PAC'95), Dallas, Texas, USA, 1–5 May 1995, pp. 1245–1247.

M. Giovannozzi *et al.*, Design and tests of a low-loss multi-turn ejection for the CERN PS, 39th ICFA Advanced Beam Dynamics Workshop: High Intensity High Brightness Hadron Beams (HB2006), Tsukuba, Japan, 29 May–2 June 2006, pp. 192–196.

M.J. Barnes, E.W. Blackmore, G.D. Wait, J. Lemire-Elmore (UBC), B. Rablah, G. Leyh, M. Nguyen and C. Pappas, Analysis of high power IGBT short circuit failures, *IEEE Trans. Plasma Sci.*, **33** (2005) 1252.

T.S. Mattison, R.L. Cassel, A.R. Donaldson and G.Gross, Fast and reliable kicker magnets for the SLC damping rings, Proc. 16th Particle Accelerator Conference (PAC'95), Dallas, Texas, USA, 1–5 May 1995, pp. 1915–1917.

D. Qunell, C. Jensen, D. Tinsley, Kicker system for 8 GeV proton injection, Proc. 17th Particle Accelerator Conference (PAC'97), Vancouver, Canada, May 12–16, 1997, pp1287–1289.

A. Ueda, T. Ushiku and T. Mitsuhashi, Construction of travelling wave kicker magnet and pulse power supply for the KEK-photon factory storage ring, Proc. 19th Particle Accelerator Conference (PAC'01), Chicago, USA, 18–22 June 2001, pp. 4050–4052.

H. Hahn, N. Tsoupas and J.E. Tuozzolo, The RHIC injection kicker, Proc. 17th Particle Accelerator Conference (PAC'97), Vancouver, Canada, 12–16 May 1997, pp. 213–215.

H. Hahn, W. Fischer, V.I. Ptitsyn and J.E. Tuozzolo, All-ferrite RHIC injection kicker, Proc. 19th Particle Accelerator Conference (PAC'01), Chicago, USA, 18–22 June 2001, pp. 3705–3707.

H. Hahn, W. Fischer, Y.K. Semertzidis and D.S. Warburton, Up-graded RHIC injection kicker system, Proc. 20th Particle Accelerator Conference (PAC'03), Portland, Oregon, USA, 12–16 May 2003, pp. 1625–1627.

C.C. Jensen and G.E. Krafczyk, NuMi Proton Kicker Extraction System, Proc. 21st Particle Accelerator Conference (PAC'05), Knoxville, Tennessee, USA, 16–20 May 2005, pp. 692–694.

M.J. Barnes, Optimize SPICE models to accurately simulate frequency-dependent impedances, *Personal Engineering & Instrumentation News*, December 1996.

M.J. Barnes and G.D. Wait, Application of ELEKTRA to the prediction of inductance distribution for a travelling wave kicker magnet, Vector Fields North American User Group Meeting, San Jose, California, 17 October 1996.

M.J. Barnes and G.D. Wait, Solid state switch alternatives for klystron modulators, Proc. 1995 Modulator/Klystron Workshop, Stanford, California, USA, 9–11 October 1995.

T. Oki, The bridged-T network lumped kicker: A novel fast magnetic kicker system for a compact synchrotron, *Nucl. Instr. Meth. Phys. Res. A: Accel., Spectr., Det. Ass. Equip.,* **607** (2009) 489.

W. Jiang, Fast High-Voltage Switching Using Stacked MOSFETs, *IEEE Trans. Dielec. Elec. Ins*., **14** (2007) 947.

T. Adachi and T. Kawakubo, *Phys. Rev. ST Accel. Beams* **16** (2013) 053501.

A. Krasnykh, Mini Kicker Workshop in ANL, Report No. SLAC-WP-096, 2013.